iScience

CellPress
OPEN ACCESS

Article

Slitrk2 deficiency causes hyperactivity with altered vestibular function and serotonergic dysregulation

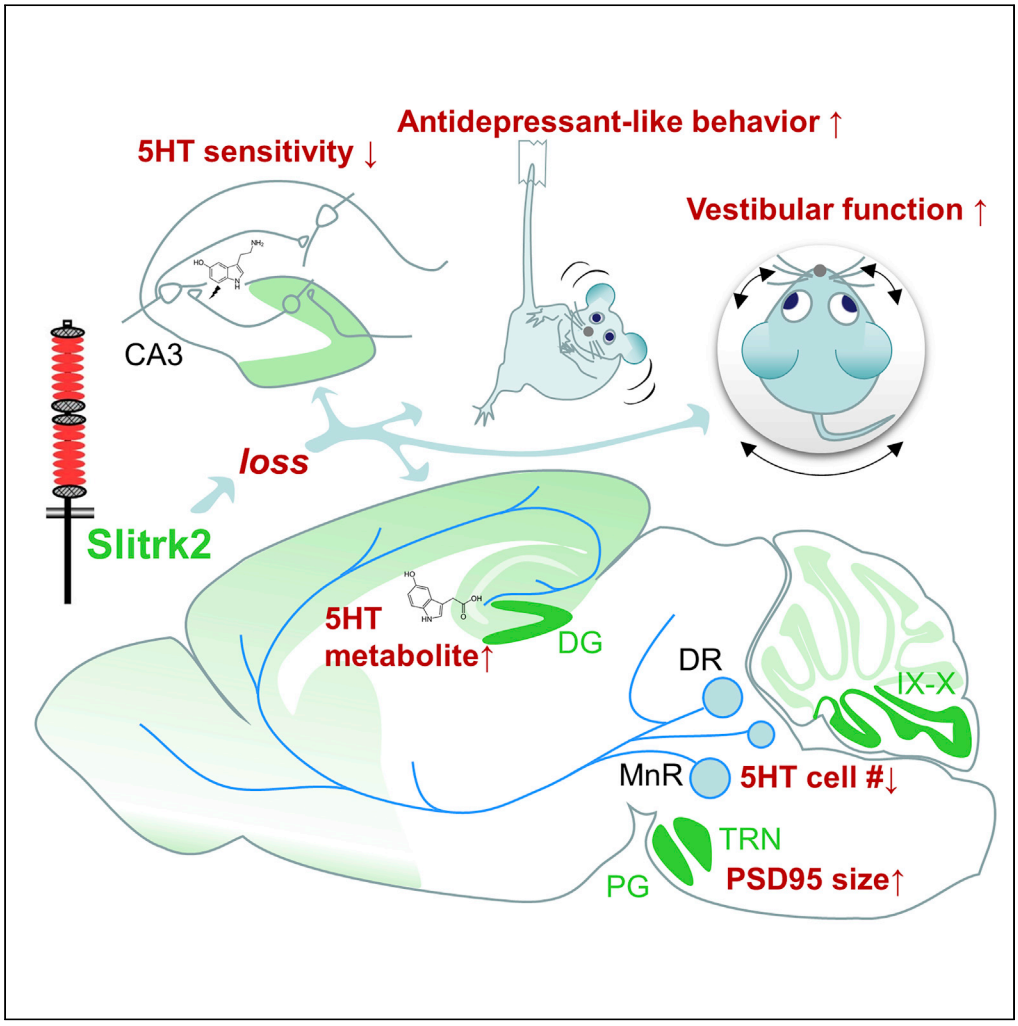

Kei-ichi Katayama, Naoko Morimura, Katsunori Kobayashi, ..., Niall P. Murphy, Soichi Nagao, Jun Aruga

aruga@nagasaki-u.ac.jp

Highlights

Slitrk2 KO mice showed antidepressant-like behaviors and enhanced vestibular function

Mossy fiber-CA3 synaptic sensitivity to serotonin was reduced in Slitrk2 KO mice

Serotonin metabolite was increased in hippocampus and amygdala of Slitrk2 KO mice

Numbers of serotonergic neurons in raphe nuclei were decreased in Slitrk2 KO mice

Katayama et al., iScience 25, 104604
July 15, 2022
https://doi.org/10.1016/j.isci.2022.104604

iScience

CellPress
OPEN ACCESS

Article

Slitrk2 deficiency causes hyperactivity with altered vestibular function and serotonergic dysregulation

Kei-ichi Katayama,[1] Naoko Morimura,[1] Katsunori Kobayashi,[2] Danielle Corbett,[3] Takehito Okamoto,[4] Veravej G. Ornthanalai,[5] Hayato Matsunaga,[6] Wakako Fujita,[6] Yoshifumi Matsumoto,[1] Takumi Akagi,[7] Tsutomu Hashikawa,[7] Kazuyuki Yamada,[8] Niall P. Murphy,[5] Soichi Nagao,[4] and Jun Aruga[1,6,9,*]

SUMMARY

SLITRK2 encodes a transmembrane protein that modulates neurite outgrowth and synaptic activities and is implicated in bipolar disorder. Here, we addressed its physiological roles in mice. In the brain, the Slitrk2 protein was strongly detected in the hippocampus, vestibulocerebellum, and precerebellar nuclei—the vestibular-cerebellar-brainstem neural network including pontine gray and tegmental reticular nucleus. Slitrk2 knockout (KO) mice exhibited increased locomotor activity in novel environments, antidepressant-like behaviors, enhanced vestibular function, and increased plasticity at mossy fiber–CA3 synapses with reduced sensitivity to serotonin. A serotonin metabolite was increased in the hippocampus and amygdala, and serotonergic neurons in the raphe nuclei were decreased in Slitrk2 KO mice. When KO mice were treated with methylphenidate, lithium, or fluoxetine, the mood stabilizer lithium showed a genotype-dependent effect. Taken together, Slitrk2 deficiency causes aberrant neural network activity, synaptic integrity, vestibular function, and serotonergic function, providing molecular-neurophysiological insight into the brain dysregulation in bipolar disorders.

INTRODUCTION

In mammals, the Slitrk family consists of six transmembrane proteins (Slitrk1–Slitrk6) that modulate neurite outgrowth and enhance synaptogenesis (Aruga and Mikoshiba, 2003; Aruga et al., 2003; Takahashi et al., 2012; Yim et al., 2013). Accumulating evidence indicates that Slitrk family proteins play various pathological roles in the brain functions. *SLITRK1* is associated with obsessive-compulsive and related disorders (Stein et al., 2019)—Tourette's syndrome (Abelson et al., 2005), trichotillomania (Zuchner et al., 2006), and obsessive compulsive disorders (OCD) (Melo-Felippe et al., 2019; Ozomaro et al., 2013)—and *Slitrk1*-deficient mice exhibit anxiety-like behaviors (Katayama et al., 2010). In addition, *LacZ*-inserted-*Slitrk5*-deficient mice exhibit OCD-like abnormalities (Shmelkov et al., 2010). Moreover, *SLITRK6* is associated with myopia and sensory deafness comorbidity (Tekin et al., 2013) and *Slitrk6* is essential for inner ear innervation (Katayama et al., 2009; Matsumoto et al., 2011).

In contrast to the aforementioned Slitrk proteins, the roles of Slitrk2 in higher brain functions are unclear. *SLITRK2*, located nearly in an X chromosomal locus, is associated with bipolar disorder (Smith et al., 2009). Moreover, in schizophrenia patients, a missense mutation leads to loss-of-function in *SLITRK2* (Kang et al., 2016; Piton et al., 2011). In terms of expression and molecular function, Slitrk2 and Slitrk1 exhibit distinct characteristics (Aruga and Mikoshiba, 2003). *Slitrk2* is highly expressed in immature neural progenitor cells, as well as in mature cells of the CNS, and overexpression of Slitrk2 inhibits nerve growth factor-induced neurite outgrowth in PC12 cells (Aruga and Mikoshiba, 2003). Slitrk2 increases synapse numbers (synaptogenic activity) through its interaction with protein tyrosine phosphate receptors (Linhoff et al., 2009; Takahashi and Craig, 2013) in addition to controlling excitatory synapse development through its interaction with membrane associated guanylate kinases such as PSD-95 (Han et al., 2019; Loomis et al., 2020). Slitrk2 levels have been shown to be reduced in the neural cells of myotonic dystrophy patients and brain *ex vivo*

[1]Laboratory for Behavioral and Developmental Disorders, RIKEN Brain Science Institute (BSI), Wako-shi, Saitama 351-0198, Japan

[2]Department of Pharmacology, Nippon Medical School, Bunkyo-ku, Tokyo 113-8602, Japan

[3]Neurotherapeutics Research Group, School of Biomolecular and Biomedical Sciences, Conway Institute, University College Dublin, Dublin 4, Ireland

[4]Laboratory for Motor Learning Control, RIKEN Brain Science Institute (BSI), Wako-shi, Saitama 351-0198, Japan

[5]Neuronal Circuit Mechanisms Research Group, RIKEN Brain Science Institute (BSI), Wako-shi, Saitama 351-0198, Japan

[6]Department of Medical Pharmacology, Nagasaki University Institute of Biomedical Sciences, Nagasaki 852-8523, Japan

[7]Support Unit for Neuromorphological Analysis, RIKEN Brain Science Institute (BSI), Wako-shi, Saitama 351-0198, Japan

[8]Support Unit for Animal Experiments, RIKEN Brain Science Institute (BSI), Wako-shi, Saitama 351-0198, Japan

[9]Lead contact

*Correspondence: aruga@nagasaki-u.ac.jp

https://doi.org/10.1016/j.isci.2022.104604

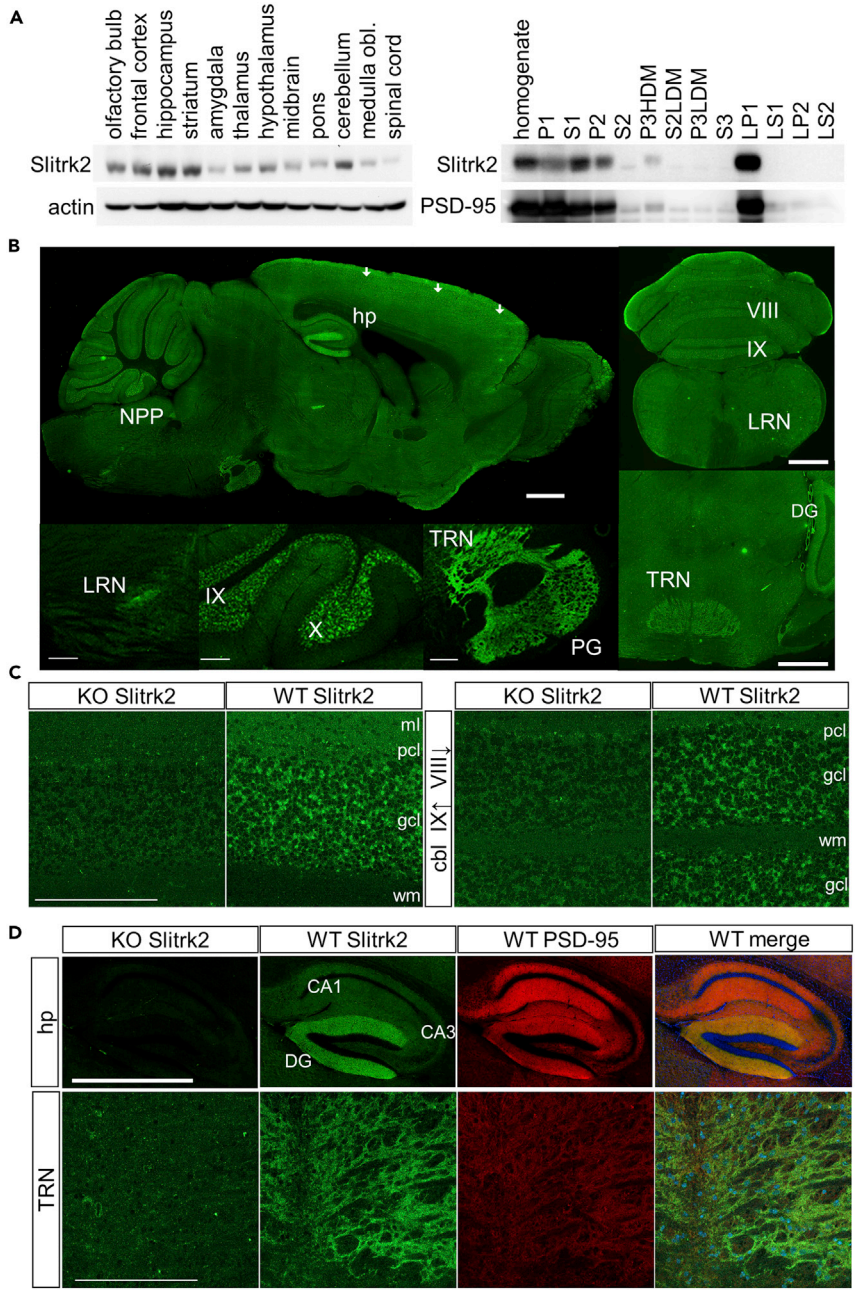

Figure 1. Distribution of Slitrk2 protein

(A) Immunoblot analysis was performed using antibodies against Slitrk2, actin, and PSD-95. In each lane, 5 μg of protein was electrophoresed. (*left top*) Distribution of Slitrk2 protein in the adult CNS. (*left bottom*) Distribution of actin as a reference. (*right top*) Subcellular distribution of Slitrk2 protein. (*right bottom*) Subcellular distribution of PSD-95 protein as a reference. Mouse brain lysate was biochemically fractionated. P1, cell nuclei and debris; P2, crude synaptosome; P3HDM, fraction enriched with Golgi apparatus; P3LDM, microsome fraction enriched with ER and transport vesicles; LP1, synaptosomal membrane; LS1, synaptic vesicle and synaptosomal cytosol; LP2, synaptic vesicle; LS2, soluble synaptosomal fraction.

(B) Immunostaining of Slitrk2. *Arrows* indicate nonspecific signals in the cerebral cortex that remained in the Slitrk2 KO brain (Figure S2).

(C) Coronal sections through 9th (IX, *left*) and 8th (VIII, *right*) lobules of the cerebellar vermis from WT and Slitrk2 KO immunoreacted with anti Slitrk2.

Figure 1. *Continued*

(D) Co-immunostaining of Slitrk2 and PSD-95. Sagittal sections (hp) or coronal sections (TRN) from WT and Slitrk2 KO mice immunoreacted with anti-Slitrk2 (*green*) and anti-PSD-95 (*red*) antibodies. DG, hippocampus dentate gyrus; hp, hippocampus; LRN, lateral reticular nucleus; NPP, nucleus prepositus; PG, pontine gray; TRN, tegmental pontine reticular nucleus; VIII, IX, X, cerebellar lobules. Thin scale bars, 200 μm; thick scale bars, 1 mm. See also Figures S1, S2, and S10.

tissue, and rescued expression of Slitrk2 recovered the neurite outgrowth deficits in patient-derived cells (Marteyn et al., 2011). However, little is known regarding the role of Slitrk2 at the individual level.

Hence, we investigated the role of Slitrk2 in brain using animal models. In this study, we clarified the Slitrk2 protein distribution, analyzed *Slitrk2* knockout (KO) mice phenotypes, and evaluated the effect of drugs on behavioral abnormalities in KO mice. The results revealed that *Slitrk2* plays essential roles in synaptic plasticity through control of the serotonergic systems.

RESULTS

Slitrk2 protein expression

First, we performed immunoblot analysis using an anti-Slitrk2 antibody to examine the distribution of Slitrk2 protein in the brains of adult male mice. Slitrk2 was ubiquitously detected in the CNS and was abundant in the hippocampus, striatum, frontal cortex, and cerebellum (Figure 1A). Among subcellular fractions, Slitrk2 protein was detected in the synaptosomal membrane fraction (LP1, Figure 1A). Strong immunofluorescence signals were observed in the molecular layer of the hippocampal dentate gyrus, granule cell layer of cerebellar lobule IX and X, pontine gray, tegmental reticular nuclei (TRN), lateral reticular nuclei, and nucleus prepositus hypoglossi (Figures 1B–1D). In the hippocampus and TRN, the immunopositive signals well overlapped with the signals of an excitatory postsynaptic protein PSD-95 (Figure 1D). Overall protein distribution profiles were consistent with the Slitrk2 mRNA distribution (Figure S1) (Lein et al., 2007).

Slitrk2 KO mice displayed hyperactivity

To clarify the role of *Slitrk2*, we generated *Slitrk2* null mutation (*Slitrk2*$^{-}$) allele (Figure S2) and investigated the phenotypes of *Slitrk2*$^{-/Y}$ (Slitrk2 KO) mice. Slitrk2 KO mice were born in an expected Mendelian ratio and no clear differences were noted in body weight change during development or in gross histological architecture of the brain (Figure S2).

Thereafter, we conducted a series of behavioral analyses to assess the role of Slitrk2 in higher brain functions (Table 1). Pronounced behavioral changes in Slitrk2 KO mice were hyperactivity accompanied by locomotion in several behavioral tests (Figure 2, Table 1). The daily locomotor activity of Slitrk2 KO mice was higher than that of wild-type (WT) mice in the home cages during the light and early dark phases (Figure 2A). In an open field test, the total distance traveled by Slitrk2 KO mice was longer than that traveled by WT mice (Figures 2B and 2C). Marked hyperactivity was observed in the initial 5 min of the 15-min observation period (Figure 2B). Movement analysis in the open field test indicated that high horizontal locomotor activity reflected both higher moving speed and longer movement duration in the testing period (Figure 2C). However, the number of movement episodes decreased, which may have been countered by the strong increase in duration per movement (Figure 2C). The enhanced locomotion activities were seen in other behavioral tests such as the elevated plus maze test (Figure 2D), light–dark box test (Figure 2E), marble burying test (Figure 2F), hole board test (Figure 2G), and social preference test (Figure S3). A significant decrease in the time spent in the center was noted in the first 2 min of the open field test (bin 1, $p = 0.0062$; bin 2, $p = 0.023$; Figure 2B), and latency to investigate the hole was decreased in the hole board test (Figure 2G). In addition, the number of marbles buried was significantly reduced in the marble burying test (Figure 2F). Overall, no clear alterations in anxiety-like behaviors such as time spent in open arms in the elevated plus-maze test (Figure 2D) and time spent in light box in the light–dark box test (Figure 2E) were noted; these results could be regarded as the altered exploratory or aversive responses to the novel environments or objects.

Furthermore, Slitrk2 KO mice displayed antidepressant-like behaviors such as decreased immobility time in both tail suspension and forced swim tests (Figure 2H). The antidepressant-like behavior was also supported by a sucrose preference test where Slitrk2 KO mice tended to show more preference to sucrose solution than WT mice (Figure S3). In the rotarod test, the latency to fall off from the rotating rod was increased in the Slitrk2 KO mice (Figure 2I), indicating that motor coordination abilities of Slitrk2 KO were better than those of WT mice. We observed back and forth turning and rearing of Slitrk2 KO mice

Table 1. Summary of Slitrk2 KO behavioral tests

behavioral test	Parameters	changes	p values	BH	test for stat.	WT *n*	KO *n*	group-order
Home cage activity								A-1
	total (24 h, bin = 1 h)	increased	§§§		RMANOVA	10	10	
	light cycle (12 h, bin = 1 h)	increased	***, §§§		RMANOVA	10	10	
	dark cycle (12 h, bin = 1 h)	increased	§§§		RMANOVA	10	10	
Open field								A-2
(in 60 × 60 cm 70 lx open field)	distance per bin (15 min, bin = 1 min)	increased	***, §§		RMANOVA	10	10	
	total distance	increased	***	sig	t-test	10	10	
	moving speed	increased	***	sig	t-test	10	10	
	duration per movement	increased	***	sig	t-test	10	10	
	distance per movement	increased	***	sig	t-test	10	10	
	movement episode No.	decreased	***	sig	t-test	10	10	
	%center per bin (15 min, bin = 1 min)	decreased	§§		RMANOVA	10	10	
	%center	decreased	0.053		t-test	10	10	
Light-dark box								A-3
	total distance	increased	**		t-test	10	10	
	%dist in L-box		n.s.		U-test	10	10	
	%time in L-box		n.s.		U-test	10	10	
	transition No.		n.s.		t-test	10	10	
	latency to enter dark box		n.s.		t-test	10	10	
Elevated plus maze								A-4
	total distance	increased	*		t-test	10	10	
	%time open		n.s.		U-test	10	10	
	%No. open		n.s.		U-test	10	10	
Startle response								B
	startle (initial/final)		n.s.		RMANOVA	15	15	
	Threshold		n.s.		RMANOVA	15	15	
	PPI		n.s.		RMANOVA	15	15	
Fear conditioning								A-5
	conditioning (%freezing after two US-CS)	decreased	***	sig	U-test	10	10	
	context test (mean %freezing)		n.s.		U-test	10	10	
	cued test							
	basal (mean %freezing)		n.s.		U-test	10	10	
	cue (mean %freezing)	decreased	0.096		U-test	10	10	
Water maze								C
	Latency		n.s.		RMANOVA	14	15	
	Distance		n.s.		RMANOVA	14	15	
	probe test							
	quadrant analysis: only target n.s.		n.s.		U-test	14	15	
	crossing analysis: only target n.s.		n.s.		RMANOVA	14	15	
Tail suspension								D-1
	%immobility	decreased	**		U-test	8	8	

(*Continued on next page*)

Table 1. *Continued*

behavioral test	Parameters	changes	p values	BH	test for stat.	WT *n*	KO *n*	group-order
Forced swimming								D-2
	%immobility	decreased	*		U-test	12	9	
Grip strength								E-3
	maximal of three trials		n.s.		t-test	10	10	
Wire hanging								E-4
	latency to fall off		n.s.		t-test	10	10	
Hole board								E-2
	distance per bin (4 min, bin = 1 min)	increased	*, §§		RMANOVA	10	10	
	total distance	increased	*		t-test	10	10	
	total movement duration	increased	*		t-test	10	10	
	latency to dip	decreased	*		t-test	10	10	
	head dip No.		n.s.		t-test	10	10	
	head dip duration		n.s.		t-test	10	10	
Rotarod								F-3
	latency to fall off (Day2, 3 trials)	increased	**		RMANOVA	9	7	
Marble burying								F-4
	buried marbles	decreased	*		U-test	10	10	
	Habituation							
	horizontal activity	increased	**	sig	t-test	10	10	
	Rearing	increased	**	sig	t-test	10	10	
Sucrose preference								G
	water intake		n.s.		t-test	12	11	
	sucrose intake	increased	**		t-test	12	11	
	sucrose preference index	increased	0.086		t-test	12	11	
Social interaction								E-1, F-1
(in 50 × 50 cm 70 lx open field)	contact No.		n.s.		t-test	10	10	
	duration of contact		n.s.		t-test	10	10	
Social preference								F-2
(in 50 × 50 cm 70 lx open field)	empty cage		n.s.		t-test	10	10	
	mouse cage		n.s.		t-test	10	10	
	preference index		n.s.		t-test	10	10	
	distance per bin (10 min, bin = 1 min)	increased	**, §§		RMANOVA	10	10	
	total distance	increased	**		t-test	10	10	
	moving speed	increased	*		t-test	10	10	
	duration per movement	increased	**		t-test	10	10	
	distance per movement	increased	**		t-test	10	10	
	movement episode No.	decreased	**		t-test	10	10	
Balance beam								H
	latency to walk across 5 mm width beam	decreased	**		t-test	15	14	

(*Continued on next page*)

Table 1. *Continued*

behavioral test	Parameters	changes	p values	BH	test for stat.	WT *n*	KO *n*	group-order
	latency to walk across 9 mm width beam	decreased	0.068		t-test	14	15	
Eye movement								I
	vestibulo-ocular reflex (VOR)							
	gain (0.17 or 0.33 Hz)	increased	*		t-test	8	8	
	Phase		n.s.		t-test	8	8	
	optokinetic reflex (OKR)							
	Gain		n.s.		t-test	8	8	
	Phase		n.s.		t-test	8	8	
	Adaptation		n.s.		t-test	8	8	

n.s., not significant; *, $p < 0.05$; **, $p < 0.01$; ***$p < 0.001$ in t-test, U-test, or $P_{(genotype)}$ in two-way ANOVA for repeated measures (RMANOVA). §§, $p < 0.01$; §§§, $p < 0.001$ in $P_{(genotype \times time\text{-}bin)}$ in RMANOVA. *sig*, significant differences in Benjamini-Hochberg (*BH*) post-hoc tests for forty t-test subjects or for twelve U-test subjects. *group-order*, name (A-I) for independent animal cohorts and the order of behavioral tests for groups subjected to multiple tests. See also Figures 2, S3, and S4.

on the rotating rod (Figure 2I and Video S1); however, they could remain on the rotating rod despite these extra movements. Parameters related to muscle strength (grip strength and wire hanging) were not significantly different between WT and Slitrk2 KO mice (Table 1).

In terms of cognitive function assessment, we performed social behavior tests (Figure S3), Morris's water maze test (Figure S4), and classical fear conditioning test (Figure S4). Although social behaviors were comparable between WT and Slitrk2 KO mice, marginal difference was observed in the cue test of fear conditioning test (Figure S4). However, the results were difficult to interpret because of the hyperactivity of Slitrk2 KO, as suggested by a lower freezing response during fear conditioning.

Overall, these results robustly revealed that Slitrk2 KO mice show hyperactivity in novel environments and antidepressant-like behaviors. It was difficult to assess the learning or memory-associated brain function using conventional behavioral tests.

Vestibular function was altered in Slitrk2 KO mice

Among the hyperactivity-related behaviors of Slitrk2 KO mice, back and forth turning on rotarod attracted our attention because such behavior is seldom observed in the rotarod test. Based on this behavior, we hypothesized that an altered vestibular function is critical for maintaining postural stability. To evaluate the vestibular function, we performed additional tests used for assessing vestibular function of mice (Ito and Nagao, 1991; Tung et al., 2014; Yamaoka et al., 2018) (Figure 3). First, we performed a balance beam test using a horizontally placed beam with a width of 9 or 5 mm, in which we measured the time required to walk across the beam. The result showed that Slitrk2 KO mice required less time to walk across the beam than WT mice (9 mm, −45%, $p = 0.067$; 5 mm, −31%, $p = 0.0029$) with higher hindlimb slipping tendency (5 mm, +89%, $p = 0.078$) (Figure 3A). Second, we measured eye movements induced by horizontal rotation in the dark (horizontal vestibulo-ocular reflex [VOR]). The horizontal optokinetic response (OKR), which shares the same neural circuit within the cerebellum as the VOR, was measured as the reference. No clear differences were noted in OKR gains and phases between WT and Slitrk2 KO mice (Figures 3B and 3C). However, Slitrk2 KO mice showed significantly increased VOR gains at the frequency of 0.17 or 0.33 Hz (Figure 3D). VOR phase was unaltered in WT and Slitrk2 KO mice (Figure 3E). The adaptation of OKR after 1 h of training, which depends on cerebellar function (Ito and Nagao, 1991), was comparable between WT and Slitrk2 KO mice (Figure 3F). Thus, the aforementioned findings indicated that vestibular function was enhanced in Slitrk2 KO mice.

Hippocampal synapse property was altered in Slitrk2 KO mice

Strong Slitrk2-like immunostaining signal was observed in the hippocampal dentate gyrus and locomotor activity correlated with output mossy fiber synaptic transmission (Kobayashi et al., 2006); hence, we

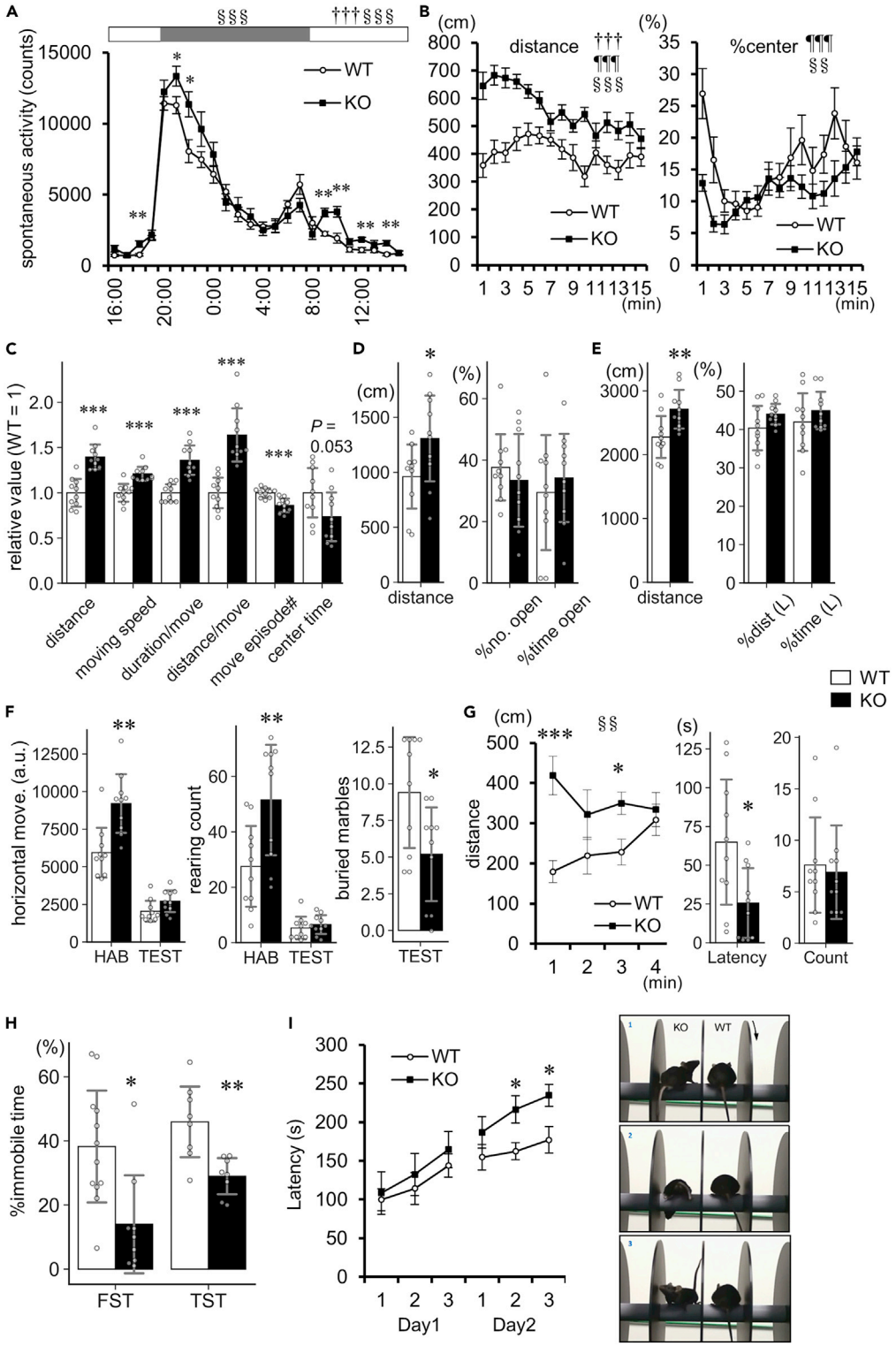

Figure 2. Behavioral phenotypes of Slitrk2 KO mice

(A) Spontaneous activities in home cages. *open box*, light-phase (8:00-20:00); *shaded box*, dark-phase (20:00-8:00). Error bars, SEM.

(B and C) Open field test. Mice were placed in an unfamiliar open field box and their movement was recorded for 15 min (B, *left*) Traveled distance in each bin. (B, *right*) Percentage time spent in the center area in each bin. Time bin = 1 min.

Figure 2. *Continued*

Error bars, SEM (C) Various parameters of the open field test were compared between WT and Slitrk2 KO mice. The mean values were adjusted to 1 in WT mice. Circles indicate values for individual mice (the same applies below).

(D) Elevated plus maze test. (*left*) Total distance traveled. (*right*) Percentages of the numbers of open arm entries to total arm entries (%no. open) and time spent in the open arm (% time open).

(E) Light–dark box test. (*left*) Total distance traveled. (*right*) Percentages of distance traveled in the light box to total distance traveled (%dist. [L]) and time spent in the light box (% time [L]).

(F) Marble burying test. The test consisted of a 30-min habituation session (HAB) and 10-min marble burying test session (TEST). In each session, horizontal movement (horizontal move.) and rearing event (rearing count) were quantified. In the marble burying test session, the number of marbles buried out of 15 marbles was counted.

(G) Hole board test. Mice were placed in a box with four holes with poke sensors for 4 min (*left*) Traveled distance in each time bin (1 min). Error bars, SEM (*middle*) Latency for the first hole investigation. (*right*) Count of total head dips (hole investigation).

(H) Immobility time in forced swim test (FST) and tail suspension test (TST). Percentages of immobile time to the total test time (5 min) are indicated.

(I) Rotarod test. (*left*) Latency to fall off the rotating rod on day 1 and day 2, the first three trials are indicated. The entire test consisted of 16 trials that were performed for 4 consecutive days (four trials/day). Error bars, SEM (*right*) Back and forth turning was observed in five of ten Slitrk2 KO mice at day 3. Images were captured after intervals of a few seconds. The movement is shown in Video S1. Data are presented as means ± SD, except A, B, G (*left*), and I where error bars represent SEM. *, $p < 0.05$; **, $p < 0.01$, ***, $p < 0.001$ in *t*-test. †††, $P_{(genotype)} < 0.001$; ¶¶¶, $P_{(time)} < 0.001$; §§§, $P_{(genotype \times time)} < 0.001$; in two-way repeated-measures ANOVA(time and genotype as main factors). Numbers of mice (n) for each experiment are shown in Table 1. See also Figures S3 and S4.

examined synaptic properties of the dentate gyrus granule cells in Slitrk2 KO mice (Figure 4A). We found no significant differences in perforant path-granule cell synapse transmission including input-output relationship, paired-pulse ratio, and long-term potentiation (LTP) between WT and Slitrk2 KO mice (Figures 4B–4D). Thereafter, we examined the electrophysiological properties of mossy fiber–CA3 pyramidal cell synapse. No significant difference was found in basal transmission efficacy or paired-pulse ratio between WT and Slitrk2 KO mice (Figures 4E and 4F). It is known that low-frequency stimulation strongly enhances transmission of this synapse, which is termed frequency facilitation (Henze et al., 2000). The frequency facilitation of mossy fiber synaptic transmission was significantly increased at 1 Hz (+15%, $p = 0.035$) in Slitrk2 KO (Figures 4G and 4H). In addition, we investigated the effects of serotonin because serotonin-induced modulation at the mossy fiber synapse was implicated in the regulation of locomotor activity (Kobayashi et al., 2008) and serotonin metabolite levels were altered in the Slitrk2 KO hippocampus as described in the following lines. In WT mice, both 1 μM and 5 μM serotonin application potentiated mossy fiber synaptic transmission (Figures 4I and 4J). In Slitrk2 KO mice, the magnitude of serotonin-induced potentiation was significantly lower than that in WT mice at both concentrations (1 μM, −44%, $p = 0.0095$; 5 μM, −20%, $p = 0.041$) (Figures 4I and 4J). Overall, we concluded that the mossy fiber–CA3 synapse transmission and pharmacological action of serotonin on the synapse transmission was affected by Slitrk2 deficiency.

Synapse morphology was mildly affected in Slitrk2 KO mice

Having seen the functional alteration of mossy fiber-CA3 synapses, we investigated the synapse morphology. Because Slitrk2 is known to bind PSD-95 (Han et al., 2019; Loomis et al., 2020), immunostaining analysis was performed to examine the PSD-95 distribution in the Slitrk2 KO brain (Figures 5A and 5B) As a presynaptic marker, VGlut1 was simultaneously detected. In the analysis of PSD-95$^+$, VGlut1$^+$, or PSD-95$^+$VGlut1$^+$-immunopositive punctate signals, we observed an increase of the PSD-95$^+$ particle sizes in TRN (+2.6%, $p = 0.044$, $n = 7$ mice per genotype, $p = 4.4 \times 10^{-5}$ $n = 56$ images from seven mice per genotype) and in pontine nuclei (+2.5%, $p = 0.067$, $n = 7$ mice per genotype, $p = 9.3 \times 10^{-5}$, $n = 56$ images from seven mice per genotype)(Figure 5 and Table S2). Similarly, PSD-95$^+$VGlut1$^+$ particle sizes in pontine gray and TRN increased (Figure 5 and Table S2). PSD-95$^+$ signal intensity was increased in pontine gray (+3.4%, $p = 0.026$, $n = 56$ images from 7 mice per genotype). In hippocampus, we observed a marginal increase of the CA1 signal intensity (+1.7%, $p = 0.017$, $n = 48$ or 56 images from 6 or 7 mice per genotype) (Figure 5 and Table S2). On the other hand, we did not see clear genotype-dependent differences of any particle counts or any parameters for VGlut1 punctate signals in either region (Figures 5A, 5B, and S5, Table S2). In agreement with the mild changes of PSD-95 distribution by immunostaining, overall content of PSD-95 as indicated by immunoblot analysis did not show significant differences in the hippocampus or in pons between WT and KO mice (Figure S5). These results indicated that Slitrk2 deficiency mildly increased PSD-95 per a synapse in TRN and pontine nuclei but had negligible effects on PSD-95 in hippocampal mossy fiber-CA3 synapses.

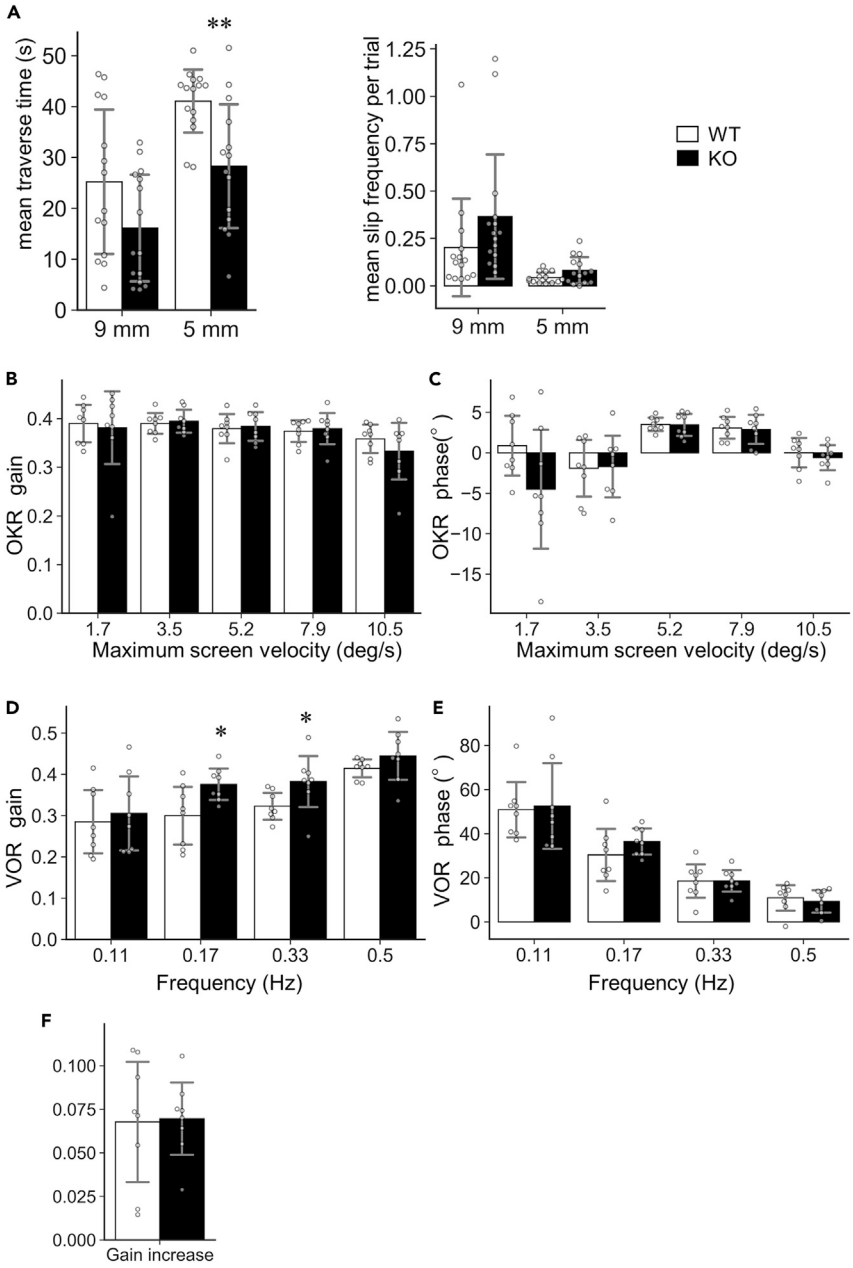

Figure 3. Vestibular function-related behaviors of Slitrk2 KO mice

(A) Balance beam test. (*left*) Mean latency (s) to walk across 50-cm horizontal bars with a width of 9 or 5 mm. (*right*) Mean frequency of slip from the bars in a trial. The tests were repeated three times.

(B and C) Dynamic characteristics of horizontal optokinetic response (OKR) of WT and Slitrk2 KO mice. (B) OKR gain. (C) OKR phases.

(D and E) Horizontal vestibulo-ocular reflex (VOR). (E) VOR gains. (E) VOR phases.

(F) Adaptation of OKR. Comparison of the increase in OKR after 1 h of training between WT and Slitrk2 KO mice. Data are presented as means ± SD. *, $p < 0.05$; **, $p < 0.01$. Numbers of mice (n) for each experiment are shown in Table 1.

To further address the CA3 synapse morphology, electron microscopic analysis was performed and determined the presynaptic and the postsynaptic parameters. No clear differences were observed in the number of postsynaptic densities (PSDs) in a synaptic terminal between WT and Slitrk2 KO mice. Both PSD length and thickness were comparable between WT and Slitrk2 KO mice (Figure 6). The mean values for the presynaptic area, synaptic vesicle density, and synaptic vesicle distances showed no obvious differences (Figure 6). However, the SD of

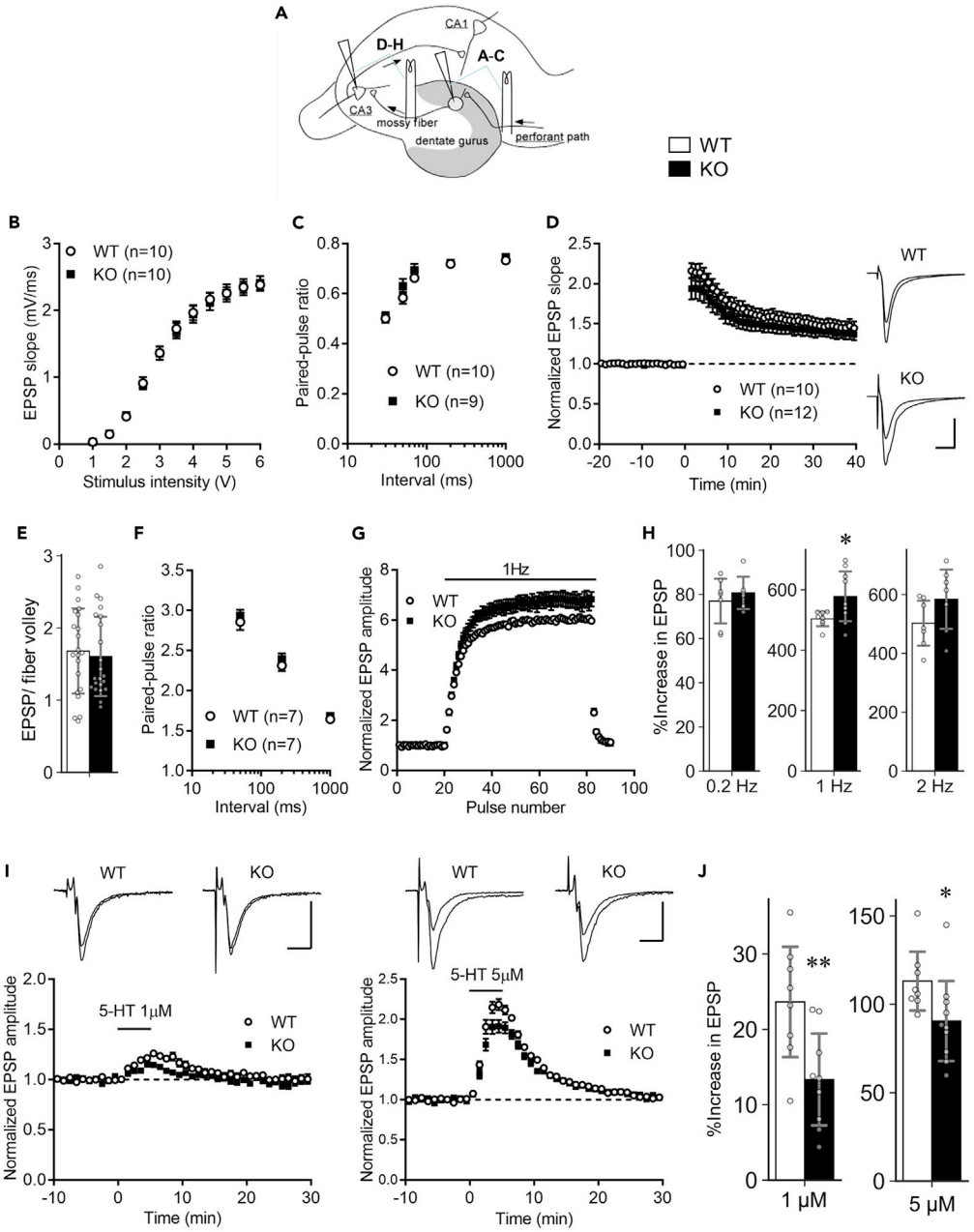

Figure 4. Electrophysiological analysis of hippocampal granule cells in Slitrk2 KO mice

(A) Schematic diagram of hippocampal excitatory neuronal circuits.

(B–D) Analyses of the medial perforant path–dentate gyrus granule cell synapse. (B) Input–output relationship. n = 10 slices from 6 mice per genotype. (C) Paired–pulse ratio. n = 10 or 9 slices from 7 mice per genotype. (D) LTP induced by tetanic stimulation delivered at 0 min. Sample recordings show averaged consecutive EPSPs at baseline and 30–40 min after the tetanic stimulation. Scale bar: 10 ms, 0.5 mV n = 10 or 12 slices from 7 or eight mice per genotype.

(E–J) Analyses of mossy fiber–CA3 synapses. (E) EPSP to presynaptic fiber volley ratio. n = 21 or 22 slices from 9 or 8 mice per genotype. (F) Paired pulse facilitation. n = 7 slices from 5 mice per genotype. (G) Time course of frequency facilitation induced by 1 Hz stimulation. (H) Summary of the magnitude of frequency facilitation induced at 0.2, 1, and 2 Hz *, p = 0.035. 0.2 Hz, n = 7 or 6 slices from 6 or 5 mice per genotype; 1 Hz, n = 8 or 9 slices from 5 or 4 mice per genotype; 2 Hz, n = 7 slices from 4 mice per genotype. (I) Modulation of mossy fiber–CA3 synaptic transmission by serotonin (5-HT) applied at 1 μM (*left*) or 5 μM (*right*) from 0 to 5 min. Sample recordings show averaged consecutive EPSPs at baseline and the peak of potentiation. Scale bar: 10 ms, 0.2 mV. (J) Summary of the magnitude of serotonin-induced synaptic potentiation. *, p = 0.0413, **, p = 0.0095. 1 μM, n = 8 or 9 slices from 4 or 5 mice per genotype; 5 μM, n = 8 or 10 slices from 8 or 9 mice per genotype. Data are presented as means ± SEM, except E, H, and J where error bars represent SD.

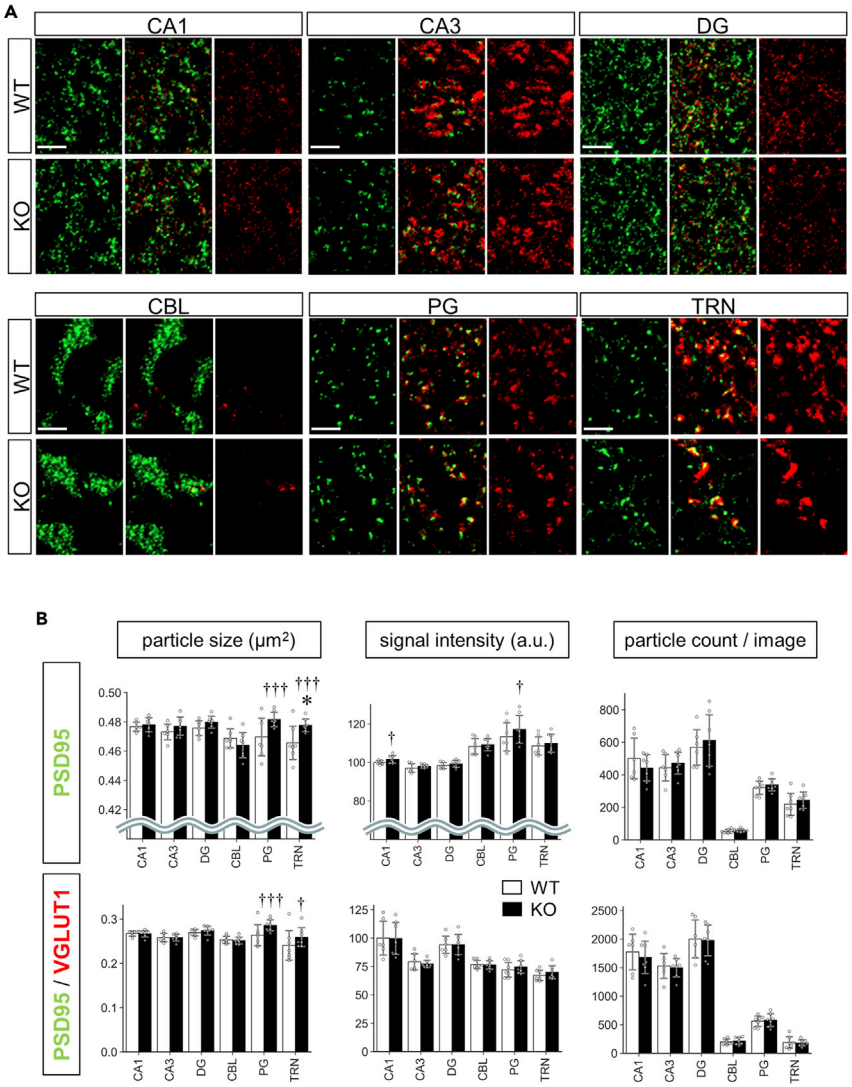

Figure 5. Quantitative analyses for PSD-95 in Slitrk2 KO brains

(A) Representative images for PSD-95 (*green*) and VGlut1 (*red*) immunostaining in the hippocampus CA1 stratum radiatum (CA1), CA3 stratum lucidum (CA3), dentate gyrus (DG), granule cell layer of Xth lobule (CBL), pontine gray matter (PG), and tegmental reticular nucleus (TRN) from the para sagittal section (lateral to 0.60–0.72 mm). Scale bars, 5 μm.

(B) Quantitative analysis of PSD-95 and VGlut1 punctate signal sizes in WT and Slitrk2 KO mice. 9–13 M-old mice were used for the analysis. Data are presented as means ± SD. *, $p < 0.05$. n = 6 or 7 mice (CA1, CA3, DG) or n = 7 mice (CBL, PG, TRN) per genotype. Independent 8 images from 4 sections were averaged for a mouse. *, $p < 0.05$. n = 6 or 7 mice (CA1, CA3, DG) or n = 7 mice (CBL, PG, TRN) per genotype. 8 images from 4 sections were averaged for a mouse. †, $p < 0.05$; †††, $p < 0.001$ in *t*-test where values for each image were used for the statistical tests (n = 48 or 56 images, Table S1). See also Table S1 and Figure S5.

synaptic vesicle distance was significantly larger in Slitrk2 KO mice than in WT mice ($p = 0.0020$ in f-test, n = 56 or 60 presynapse from 3 mice per genotype) (Figure 6), indicating the irregularity of the synaptic vesicle distribution in Slitrk2 KO mice. In addition, the synaptic cleft width was slightly increased (+4.85%, $p = 0.052$, n = 105 or 106 synapses from 3 mice per genotype) in Slitrk2 KO mice (Figure 6). These results indicated that the absence of Slitrk2 had little effect on the mossy fiber-CA3 synapse morphology.

In addition, we investigated the dendrite spine morphology of the dentate gyrus molecular layer where Slitrk2-immunopositive signals were dense. However, the quantitative analysis of Golgi-stained sections did not show clear differences in the length, width, and density of spines (Figure S6).

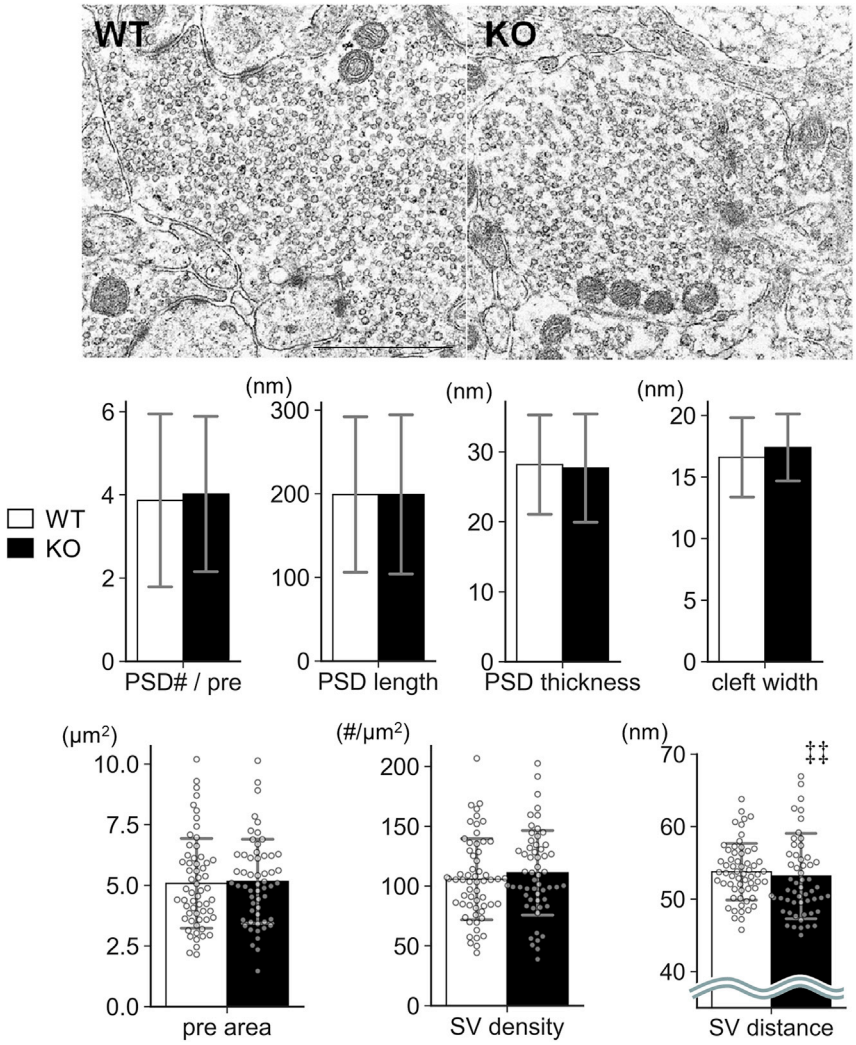

Figure 6. Electron microscopic analysis of mossy fiber–CA3 synapses in Slitrk2 KO mice

(*top*) Representative images of transmission electron microscopic analysis. Scale bar, 1 μm. (Middle from left to right) Number of PSD in a mossy fiber synaptic terminus, PSD length, PSD thickness, and cleft width. Data are presented as means ± SD. WT, n = 105 synapse from 3 mice; KO, n = 106 synapse from 3 mice. (*bottom*) Area of presynaptic terminus (unit); synaptic vesicle densities in presynaptic terminus; inter-synaptic vesicle distances. WT, n = 60 presynapse from 3 mice; KO, n = 56 presynapse from 3 mice. ‡‡, $p < 0.01$ in f-test. See also Figure S6.

Consequently, the morphological changes in Slitrk2-enriched sites were thought to be too mild to fully explain the altered behaviors and the hippocampal synaptic plasticity. We considered that Slitrk2 may have affected brain function not through conventional synaptogenesis-related protein functions of the Slitrk family but through some unrecognized mechanisms in previous studies.

Serotonergic metabolite was increased in the Slitrk2 KO brain

We then hypothesized that monoamine neurotransmitter disturbances were the basis of the hyperactivity and antidepressant-like behaviors in Slitrk2 KO mice because altered monoaminergic signaling has been associated with hyperactivity in both humans and mice (Leo and Gainetdinov, 2013; Mehta et al., 2019; Purper-Ouakil et al., 2011). We measured the levels of dopamine, serotonin, noradrenaline, and their metabolites in the prefrontal cortex, striatum, hippocampus, amygdala, and nucleus accumbens using high-performance liquid chromatography (HPLC)–electrochemical detection. Serotonin metabolite 5-hydroxyindoleacetic acid (5-HIAA) was significantly higher in the hippocampus (+22%, $p = 0.045$) and amygdala (+22%, $p = 0.030$) (Figure 7A and Table S1) and serotonin (5-HT) levels tended to be higher in

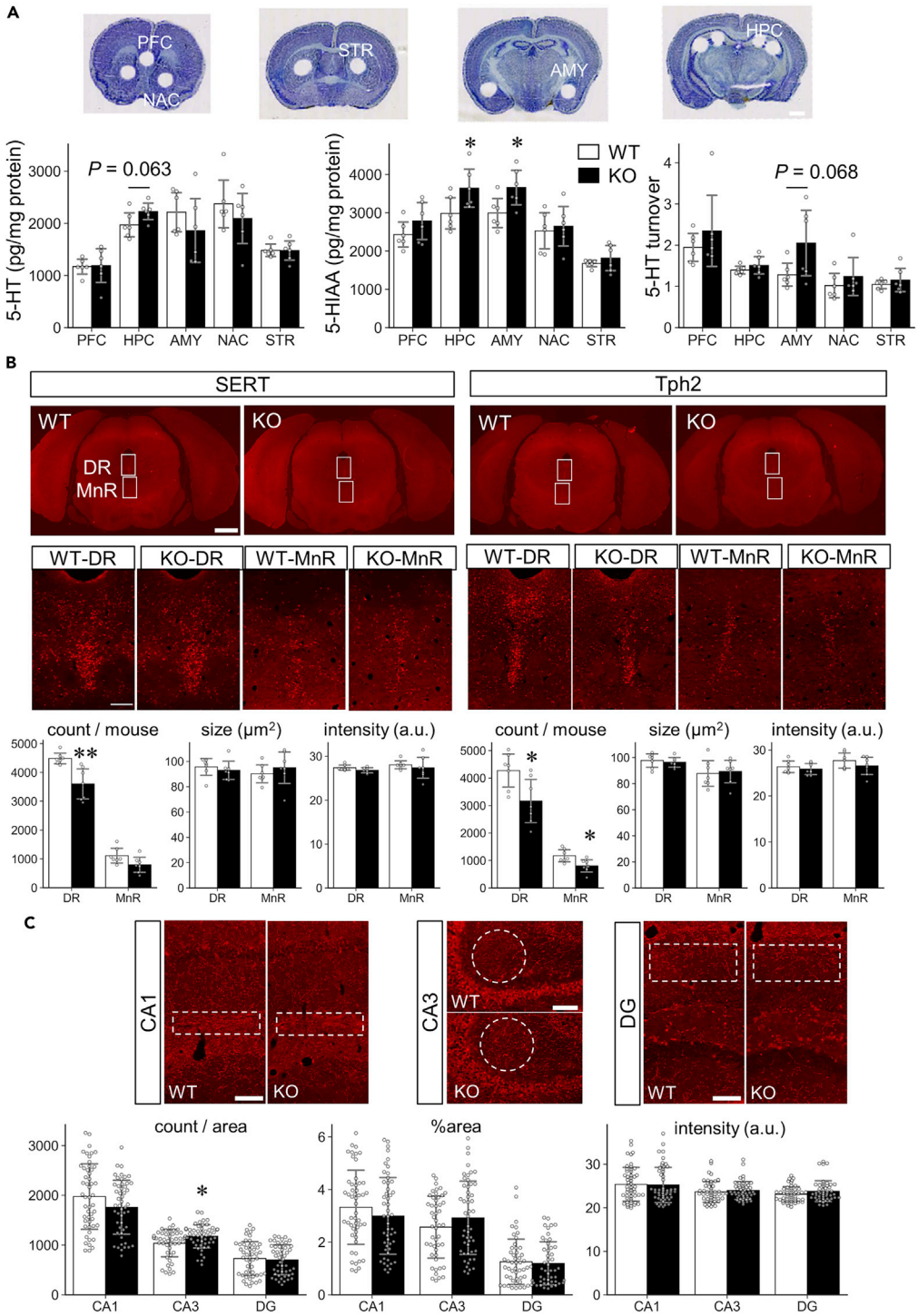

Figure 7. Serotonergic dysregulation and location of serotonergic cells

(A) Monoamine contents in Slitrk2 KO brain regions. (*top*) Each brain region was punched out from frozen brain sections. AMY, amygdala; HPC, hippocampus; NAC, nucleus accumbens; PFC, medial prefrontal cortex; STR, striatum. Scale bar, 1 mm. (*bottom*) Serotonin (5-HT) concentrations, serotonin metabolite (5-HIAA) concentrations, serotonin turnover (5-HIAA/5-HT), dopamine (DA) and its metabolites (DOPAC and HVA) concentrations; n = 6 mice per genotype.

(B) Morphometric analysis of serotonergic neurons. (*top*) Representative SERT or Tph2 immunostaining images (bregma −4.5 mm) for dorsal raphe (DR) and median raphe nuclei (MnR) from WT and Slitrk2 KO mice. The boxed regions in low magnification views are shown below. Thick scale bar, 1 mm; thin scale bar, 100 μm. (*bottom*) Estimated total particle

Figure 7. *Continued*

count per mouse (*left*), mean particle size (*middle*), and mean signal intensity of particles (*right*) were quantified. 8–10 M-old mice were used for the analysis. n = 7 mice per genotype. Values from 5 to 13 images (DR) or 3–8 images (MnR) were summed or averaged per mouse.

(C) SERT-positive fiber-like signals were quantified in hippocampal CA1 stratum lacunosum moleculare, CA3 stratum radiatum; and dentate gyrus (DG) stratum moleculare (dorsal lip). n = 48–51 images from 8 mice per genotype (4–8 images per mouse). Data are presented as means ± SD. *, $p < 0.05$; **, $p < 0.01$ in *t*-test. See also Figure S7.

the hippocampus (+13%, p = 0.063) (Figure 7A and Table S1). Serotonin turnover as defined 5-HIAA/5-HT was increased in the Slitrk2 KO amygdala (+60%, p = 0.068) (Figure 7A and Table S1). In terms of dopamine or its metabolites in Slitrk2 KO mice, a dopamine metabolite homovanillic acid (HVA) was significantly increased in the hippocampus (HVA, +24%, p = 0.048) (Table S1), but no clear differences were noted in the striatum and nucleus accumbens (Table S1). No clear differences were noted in the levels of noradrenaline in any regions (Table S1).

Serotonergic neurons were decreased in Slitrk2 KO dorsal raphe nucleus

We examined the serotonergic neurons in the Slitrk2 KO brain having seen the serotonergic dysregulation. Because the hippocampus and amygdala are known to be projected from serotonergic neurons in dorsal (B7d and B7v) and median (B8) raphe nuclei (Muzerelle et al., 2016), we performed quantitative immunostaining using anti-serotonin transporter (SERT) antibody and anti-tryptophan hydroxylase 2 (Tph2) antibody. To this end, serial sections encompassing both raphe nuclei were prepared, and immunopositive particle signals corresponding to the serotonergic cell bodies were analyzed. Consequently, compared with the WT dorsal raphe nucleus, the KO dorsal raphe nucleus contained fewer serotonergic neurons (SERT, −20%, p = 0.0020; Tph2, −26%, p = 0.018, n = 7 mice per genotype) (Figure 7B). The mean number of the KO median raphe nucleus was lower than that of WT (SERT, −28%, p = 0.055; Tph2, −31%, p = 0.014, n = 7 mice per genotype) (Figure 7B).

We then quantified the $SERT^+$ fibers in the hippocampus (Figure 7C). The signals were quantified in CA1 stratum lacunosum moleculare where dense SERT fibers were observed, CA3 stratum radiatum which is adjacent to stratum lucidum where CA3-mossy fiber synapses exist with scarce $SERT^+$ fibers, and CA3 dentate gyrus stratum moleculare where performant path-granule cell synapses exist. The results indicate that the SERT positive fiber count was increased in the CA3 region (+13%, p = 0.011, n = 49 or 50 images from 8 mice per genotype). The other regions or parameters did not show significant genotype-dependent differences.

In addition, we investigated spatial relationships between serotonergic neurons and Slitrk2 protein distribution. We performed double immunostaining analysis for serotonergic cell markers Tph2 and Slitrk2 and found that serotonergic neurons were sparsely present in TRN that expressed Slitrk2 (Figure S7). Based on the location, these serotonergic cells were considered to belong to the B9 group of serotonergic neurons (Muzerelle et al., 2016). However, we did not observe any Slitrk2-like immunopositive signals in the dorsal or median raphe nuclei in the adult mouse brain.

Hyperactivity of Slitrk2 KO mice was resistant to selected therapeutics

Hyperactivity is a clinical feature of several neuropsychiatric disorders such as attention deficit hyperactive disorders (ADHD) and bipolar disorder. Hyperactivity in ADHD patients can be attenuated by methylphenidate (American Academy of Pediatrics, 2011), and lithium is the first-line treatment to prevent manic and depressive episodes of bipolar disorder (Alda, 2015). To discern the nature of the hyperactivity exhibited by Slitrk2 KO mice, we evaluated the effects of these drugs on the locomotor activity of Slitrk2 KO mice. Acute administration of methylphenidate enhanced the locomotor activity in both WT and Slitrk2 KO mice (Figure 8A). Lithium was chronically administered to mice for 4 weeks to achieve a therapeutically relevant plasma level. The chronic lithium treatment did not significantly alter the locomotor activity, but reduced the immobility time in tail suspension test and forced swimming test in both WT and Slitrk2 KO mice (Figure 8B). Although a possibility of floor effect cannot be excluded, the effects of lithium on the tail suspension test were genotype dependent ($F [1, 56] = 8.3$, $P_{(treatment \times genotype)} = 0.0058$ in of two-way ANOVA), disposing the difference (%immobility: WT, 46%; KO, 29%; $p < 0.0001$) to a comparable level (%immobility: WT, 18%; KO, 17%; p = 0.89) (Figure 8B).

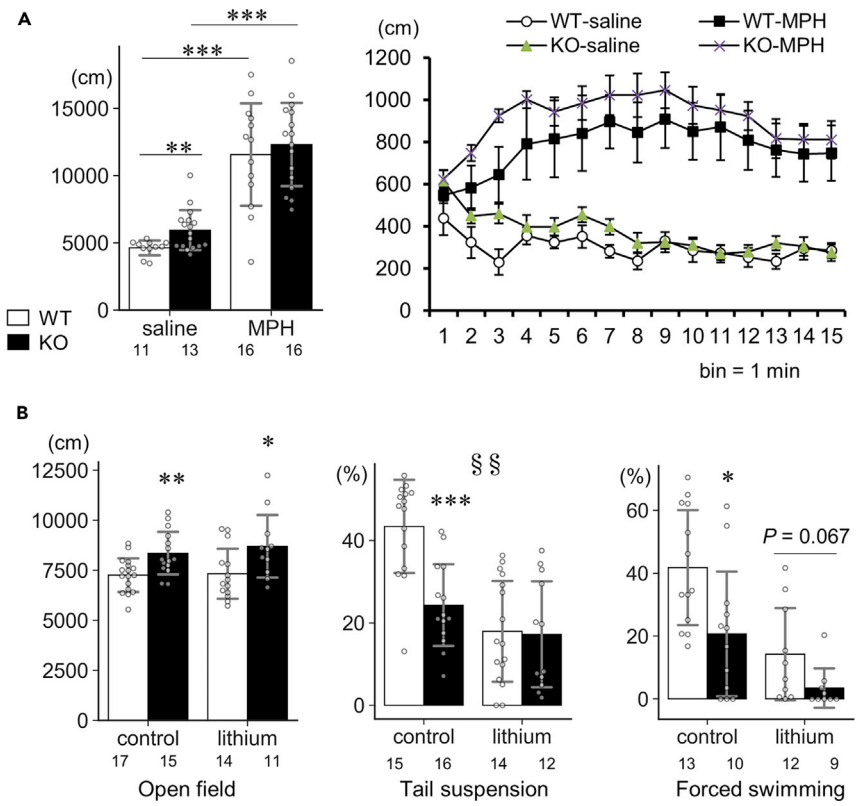

Figure 8. Effects of drugs on Slitrk2 KO mice hyperactivity

(A) Methylphenidate. Methylphenidate (5 mg/kg) was intraperitoneally administered to mice immediately before the 15-min open field test. Control mice were administered the same volume of saline. The results of total distances traveled (*left*) and distances traveled in each time bin (1 min) (*right*, Error bars, SEM).

(B) Lithium. Lithium was administered to mice at a dose of 2.4 g/kg/day through a food pellet containing lithium carbonate. After 4 weeks administration, open field test (left), tail suspension test (middle), and forced swim test (right) were performed. Control mice were fed normal food pellets without lithium carbonate. Data are presented as means ± SD, except A (*right*) where error bars represent SEM *, $p < 0.05$; **, $p < 0.01$; ***, $p < 0.001$ in *t*-test. §§, $P_{(genotype \times treat)} < 0.01$ in two-way ANOVA. Numbers of mice (n) in experimental groups are indicated below bar graphs. See also Figure S8.

In addition, we assessed the effect of selective serotonin reuptake inhibitors because current monoamine analysis indicated dysregulation of serotonin metabolism. To this end, fluoxetine was chronically administered to mice for 10 days and their spontaneous activities in home cages were compared. Chronic fluoxetine administration resulted in the reduction of activities of both WT and Slitrk2 KO mice, without the genotype-dependent differences in the reduction extent (Figure S8).

DISCUSSION

In this study, we revealed Slitrk2 protein distribution in the mouse brain and analyzed brain-associated phenotypes of Slitrk2 KO mice. Slitrk2 proteins were densely distributed in the hippocampal dentate gyrus, precerebellar nuclei, and vestibulocerebellum. The characteristic behaviors of Slitrk2 KO mice include hyperactivity in novel environments, antidepressant-like behaviors, and enhanced vestibular function. In the hippocampus, serotonin-induced synaptic modulation was reduced at the mossy fiber synapses. Serotonin metabolite levels were increased in the hippocampus and amygdala, and the numbers of serotonergic neurons in raphe nuclei were reduced. The behavioral effects of drugs targeting dopaminergic or serotonergic transmission were not altered, except that lithium diminished the difference between WT and Slitrk2 KO mice in the tail suspension test.

First, we presumed dysregulation of dopaminergic system as a basis of hyperactivity because experimental manipulation of the rodent dopaminergic system is known to induce hyperactive states and dopamine system genes are associated with hyperactivity in ADHD (Gallo and Posner, 2016; Koob et al., 1981). However,

our monoamine analysis revealed no change in dopamine or its metabolites in the nucleus accumbens, which is critical for hyperactivity caused by dopaminergic dysregulation (Koob et al., 1981). In addition, methylphenidate did not rescue the hyperactivity phenotype. Therefore, the involvement of dopaminergic dysregulation is not likely to be the major basis of the hyperactivity phenotype in Slitrk2 KO mice, although we cannot fully exclude the possibility at this point.

On the other hand, the diminished effectiveness of lithium against antidepressant-like behavior suggests that the underlying pathophysiology in Slitrk2 KO mice should be considered. Lithium is the first-line treatment for the prevention of manic and depressive episodes in bipolar disorder (Alda, 2015). Animal studies have reported that lithium increases serotonin transmission by multiple molecular mechanisms such as increased synthesis of serotonin, increased uptake of tryptophan, and increased release of serotonin (Alda, 2015). In addition to the primary action on glycogen synthase kinase 3β or second messenger systems, it is proposed that lithium induces higher-order mechanisms such as the promotion of neurogenesis in the hippocampus and stabilization of neuronal activity (Alda, 2015; Jope, 1999; Wood et al., 2004). In a recent study, hyperexcitability phenotype of young hippocampus dentate gyrus-like neurons from bipolar disorder patient-derived iPS cells was selectively reversed by lithium treatment only in neurons from patients who responded to lithium treatment (Mertens et al., 2015).

Some of the aforementioned neural targets of lithium are expected to be associated with the hyperactivity or antidepressant-like behaviors of Slitrk2 KO mice. Based on the results of the current study, the dysregulation of serotonergic signaling should be noted. Although serotonergic signaling is well recognized as a therapeutic target of many antidepressants, serotonergic signaling-associated genes such as HTR6 have been linked to bipolar disorder in a recent genome-wide association study (Mullins et al., 2021). Serotonin transporter gene (SLC6A4) has been proposed to affect response to lithium treatment among bipolar disorder patients (Senner et al., 2021). Because serotonergic signaling critically controls the excitability of neurons, Slitrk2 might be involved in the control of neuronal excitability through the serotonergic nervous system.

Involvement of serotonergic signaling in the antidepressant-like phenotypes in mice is also supported by studies using other genetically modified mice. Tph2 KO mice show hyperactivity on the exposure to novel environments, and reduced immobility in both forced swimming test and tail suspension test with altered hippocampal neuroplasticity (Maddaloni et al., 2018). Conditional KO of STAT3 in dorsal raphe nuclei reduced immobility in forced swimming test (Reisinger et al., 2021). Local neuroinflammation in dorsal raphe nuclei in interleukin 1β transgenic mice exhibited increased stress-induced locomotion (Howerton et al., 2014). These results led us to hypothesize that decreased serotonergic cell number in raphe nuclei may be related to the hyperactivity and antidepressant-like behavioral abnormalities in Slitrk2 KO mice.

Although the actual mechanism underlying the serotonergic cell decrease is yet to be clarified, the phenotype may reflect the role of Slitrk2 during development. Previous studies showed that Slitrk2 mRNA expression detected at E10.5 peaks around E13 and is detected widely in the ventral layer along the entire rostrocaudal axis in mouse embryo (Aruga and Mikoshiba, 2003) and serotonergic neurons are generated on E9.5–E12 in mice (Deneris and Gaspar, 2018). We speculate that Slitrk2 may control the generation of serotonergic neurons. This idea should be verified through extensive analysis of cell proliferation, differentiation, and cell death with spatiotemporally fine scales.

Because the serotonergic neurons in raphe nuclei send their axons widely as early as late embryonic stages, the cell number reduction may have profound effects on the establishment of local serotonergic signaling. It is known that the hippocampal serotonergic fibers are shaped in response to subtle changes of serotonin homeostasis (Nazzi et al., 2019). As to the hippocampus of Slitrk2 KO mice, serotonin and its metabolite were increased together with the increased density of the serotonergic fibers at CA3. These lines of evidence suggest the presence of excessive serotonergic signaling at CA3. Endogenous serotonin can potentiate mossy fiber-CA3 synaptic transmission (Kobayashi et al., 2020). The excessive serotonergic signaling in Slitrk2 KO may have caused the reduction of the serotonin effects on mossy fiber-CA3 synapse as observed. Because serotonin potentiates mossy-fiber CA3 synaptic transmission via presynaptic mechanisms (Kobayashi et al., 2008), long-lasting change of the serotonergic signaling tone may have caused the altered presynaptic properties such as the increased frequency facilitation and the unevenness of the synaptic vesicles, both of which were observed in Slitrk2 KO mice. In this way, the hippocampal phenotypes of Slitrk2 KO can be interpreted from the viewpoint of dysregulated serotonergic signaling.

In addition to the hyperactivity and antidepressant-like behavioral abnormalities, Slitrk2 KO mice exhibited enhanced vestibular function. In our behavioral tests, enhanced vestibular reflex eye movements (VOR) were observed in Slitrk2 KO mice. Because KO mouse OKR was intact, we consider that vestibular functional alteration in Slitrk2 KO mice mainly represented some abnormalities in the peripheral vestibular system. Accordingly, Slitrk2 is expressed in sensory neuroepithelia in developing mice (Figure S9). However, we did not see any obvious abnormalities in vestibular organs or sensory neuroepithelia of Slitrk2 KO mice in morphological analysis (Figure S9).

An intriguing point lies in the relationship between the hyperactivity and enhanced vestibular function. Bilateral vestibular deafferentation results in hyperactivity in rodents (Stiles et al., 2012). Genetic inner ear dysfunctions such as conditional Slc12a2 KO or Tbx1 KO in the inner ear (Antoine et al., 2017) and a chemically induced mutation of Myo7a (Avni et al., 2009) cause motor hyperactivity. However, whether hyperactivity is induced by the altered vestibular function has not yet been clarified. Further investigation of the role of Slitrk2 in vestibular systems is required for better understanding.

Slitrk2 KO phenotypes, as summarized before, have some clinical implications. First, some genetic studies suggest an association between SLITRK2 and bipolar disorders (Smith et al., 2009). Hyperactivity with impaired adaptive responses to novel environment or object in Slitrk2 KO mice is suggestive of the manic status of bipolar disorder. Together with the genotype-dependent antidepressant effect of lithium, it would be beneficial to further clarify the relationship between Slitrk2 function and the pathophysiology of bipolar disorder. Second, a case of a male patient with a deletion of an X chromosome region, including FMR1, FMR2, and SLITRK2, has been reported (Cavani et al., 2011). The patient showed severe mental retardation, autistic-like behavioral profile, and nystagmus (Cavani et al., 2011). The presence of nystagmus suggests an altered vestibular function, which could be because of the loss of SLITRK2. Third, the hyperactivity phenotype is a clinical feature of ADHD. It is noteworthy that significantly higher VOR gains, which we observed in Slitrk2 KO mice, were observed in ADHD and autism-spectrum-disorder patients (Van Hecke et al., 2019), and that ADHD patients show impaired balance function (Konicarova et al., 2014; Shum and Pang, 2009). Therefore, any alterations of SLITRK2 function could be present in patients with hyperactivity.

Limitations of the study

Although this study reported several phenotypes of Slitrk2 KO mice, there are gaps between the molecular function of Slitrk2 and Slitrk2 KO mice phenotypes. Concerning the synaptic phenotypes, we observed mild alterations in PSD-95 immunopositive signals in the Slitrk2 KO TRN and pontine nuclei and the morphology of mossy fiber-CA3 synapses. As an explanation of the fairly mild phenotype of a hippocampal synapse could be the functional compensation of the other members of Slitrk family proteins, such as Slitrk5, which is strongly expressed in hippocampal granule cells (Lein et al., 2007) and possesses synaptogenic activities (Takahashi and Craig, 2013; Yim et al., 2013). It is essential to clarify specific and common roles of Slitrk family genes *in vivo*, which would contribute to the better understanding of neuropsychiatric disorders. Another inherent limitation of this study is the use of conventional KO mice. The conventional KO phenotype provides us the information more comprehensively than that of conditional KO. In this study, we adopted an unbiased approach concerning the Slitrk2 protein distribution and Slitrk2 conventional KO behavioral phenotypes. This is partly because of the fact that our goal includes understanding pathophysiological caused by Slitrk2 deficiency because Slitrk2 appeared as the candidate genetic factors for some neuropsychiatric disorders. Better understanding for the neural circuit basis of the behavioral phenotypes would be obtained in prospective conditional KO studies.

STAR★METHODS

Detailed methods are provided in the online version of this paper and include the following:

- KEY RESOURCES TABLE
- RESOURCE AVAILABILITY
  - Lead contact
  - Materials availability
  - Data and code availability
- EXPERIMENTAL MODEL AND SUBJECT DETAILS
- METHOD DETAILS
  - Antibodies

- Western blot analysis
- Immunofluorescence staining
- Generation of Slitrk2-null mutant mice
- Home cage activity
- Open field test
- Elevated plus maze test
- Light-dark box test
- Marble burying test
- Hole board test
- Forced swim test
- Tail suspension test
- Sucrose preference test
- Rotarod test
- Social behavior tests
- Tests for startle response, wire hanging, and grip strength
- Water maze test and fear conditioning test
- Balance beam test
- VOR and OKR eye movements
- Electrophysiology
- Morphological analysis
- Neurochemical analysis
- Drug administration

- QUANTIFICATION AND STATISTICAL ANALYSIS

SUPPLEMENTAL INFORMATION

Supplemental information can be found online at https://doi.org/10.1016/j.isci.2022.104604.

ACKNOWLEDGMENTS

We thank Yuri S. Odaka (RIKEN) for inner ear and electron microscopic analysis, Maya Odagawa (RIKEN) for immunostaining analysis, and Noriko Takashima (RIKEN) for fluoxetine treatment analysis. This study was supported by RIKEN BSI funds, grants from the Japan Society for the Promotion of Science and MEXT (22H02722, 20K21605, 19H03327, 16H04666, 21240031, 25110736, and 18700330), and research grant from the Uehara Memorial Foundation.

AUTHOR CONTRIBUTIONS

Conceptualization, K.Ka., N.M., and J.A.; Investigation, K.Ka., N.M., K.Ko, D.C., T.O., V.G.O., H.M., W.F., Y.M., T.A., T.H., K.Y., N.P.M., S.N., and J.A.; Writing–Original Draft, K.Ka. and J.A.; Writing–Review & Editing, K.Ko., D.C., T.A., K.Y., N.P.M., S.N., and J.A.; Funding Acquisition, K.Ka., J.A.; Supervision, J.A.

DECLARATION OF INTERESTS

The authors declare no competing interests.

Received: September 23, 2021
Revised: April 14, 2022
Accepted: June 8, 2022
Published: July 15, 2022

REFERENCES

Abelson, J.F., Kwan, K.Y., O'Roak, B.J., Baek, D.Y., Stillman, A.A., Morgan, T.M., Mathews, C.A., Pauls, D.L., Rasin, M.R., Gunel, M., et al. (2005). Sequence variants in SLITRK1 are associated with Tourette's syndrome. Science *310*, 317–320. https://doi.org/10.1126/science.1116502.

Alda, M. (2015). Lithium in the treatment of bipolar disorder: pharmacology and pharmacogenetics. Mol. Psychiatr. *20*, 661–670. https://doi.org/10.1038/mp.2015.4.

American Academy of Pediatrics (2011). ADHD: Clinical practice guideline for the diagnosis, evaluation, and treatment of Attention-Deficit/Hyperactivity Disorder in children and adolescents. Pediatrics *128*, 1007. https://doi.org/10.1542/peds.2011-2654.

Antoine, M.W., Vijayakumar, S., McKeehan, N., Jones, S.M., and Hébert, J.M. (2017). The severity of vestibular dysfunction in deafness as a determinant of comorbid hyperactivity or anxiety. J. Neurosci. *37*, 5144–5154. https://doi.org/10.1523/JNEUROSCI.3545-16.2017.

Aruga, J., and Mikoshiba, K. (2003). Identification and characterization of Slitrk, a novel neuronal

transmembrane protein family controlling neurite outgrowth. Mol. Cell. Neurosci. *24*, 117–129. https://doi.org/10.1016/s1044-7431(03)00129-5.

Aruga, J., Yokota, N., and Mikoshiba, K. (2003). Human SLITRK family genes: genomic organization and expression profiling in normal brain and brain tumor tissue. Gene *315*, 87–94. https://doi.org/10.1016/s0378-1119(03)00715-7.

Avni, R., Elkan, T., Dror, A.A., Shefer, S., Eilam, D., Avraham, K.B., and Mintz, M. (2009). Mice with vestibular deficiency display hyperactivity, disorientation, and signs of anxiety. Behav. Brain. Res. *202*, 210–217. https://doi.org/10.1016/j.bbr.2009.03.033.

Cavani, S., Prontera, P., Grasso, M., Ardisia, C., Malacarne, M., Gradassi, C., Cecconi, M., Mencarelli, A., Donti, E., and Pierluigi, M. (2011). FMR1, FMR2, and SLITRK2 deletion inside a paracentric inversion involving bands Xq27.3-q28 in a male and his mother. Am. J. Med. Genet. *155*, 221–224. https://doi.org/10.1002/ajmg.a.33515.

Deneris, E., and Gaspar, P. (2018). Serotonin neuron development: shaping molecular and structural identities. WIREs Dev. Biol. *7*, e301. https://doi.org/10.1002/wdev.301.

Frankish, A., Diekhans, M., Jungreis, I., Lagarde, J., Loveland, J.E., Mudge, J.M., Sisu, C., Wright, J.C., Armstrong, J., Barnes, I., et al. (2021). Gencode 2021. Nucleic Acids Res. *49*, D916–D923. https://doi.org/10.1093/nar/gkaa1087.

Gallo, E.F., and Posner, J. (2016). Moving towards causality in attention-deficit hyperactivity disorder: overview of neural and genetic mechanisms. Lancet Psychiatr. *3*, 555–567. https://doi.org/10.1016/S2215-0366(16)00096-1.

Han, K.A., Kim, J., Kim, H., Kim, D., Lim, D., Ko, J., and Um, J.W. (2019). Slitrk2 controls excitatory synapse development via PDZ-mediated protein interactions. Sci. Rep. *9*, 17094. https://doi.org/10.1038/s41598-019-53519-1.

Henze, D.A., Urban, N.N., and Barrionuevo, G. (2000). The multifarious hippocampal mossy fiber pathway: a review. Neuroscience *98*, 407–427. https://doi.org/10.1016/S0306-4522(00)00146-9.

Howerton, A.R., Roland, A.V., and Bale, T.L. (2014). Dorsal raphe neuroinflammation promotes dramatic behavioral stress dysregulation. J. Neurosci. *34*, 7113–7123. https://doi.org/10.1523/JNEUROSCI.0118-14.2014.

Ito, M., and Nagao, S. (1991). Comparative aspects of horizontal ocular reflexes and their cerebellar adaptive control in vertebrates. Comp. Biochem. Physiol. C Comp. Pharmacol. Toxicol. *98*, 221–228. https://doi.org/10.1016/0742-8413(91)90198-3.

Jastreboff, P.J. (1979). Evaluation and statistical judgement of neural responses to sinusoidal stimulation in cases with superimposed drift and noise. Biol. Cybern. *33*, 113–120. https://doi.org/10.1007/BF00355259.

Jope, R.S. (1999). A bimodal model of the mechanism of action of lithium. Mol. Psychiatr. *4*, 21–25. https://doi.org/10.1038/sj.mp.4000444.

Kabayama, M., Sakoori, K., Yamada, K., Ornthanalai, V.G., Ota, M., Morimura, N., Katayama, K.-i., Murphy, N.P., and Aruga, J. (2013). Rines E3 ubiquitin ligase regulates MAO-A levels and emotional responses. J. Neurosci. *33*, 12940–12953. https://doi.org/10.1523/JNEUROSCI.5717-12.2013.

Kang, H., Han, K.A., Won, S.Y., Kim, H.M., Lee, Y.H., Ko, J., and Um, J.W. (2016). Slitrk missense mutations associated with neuropsychiatric disorders distinctively impair Slitrk trafficking and synapse formation. Front. Mol. Neurosci. *9*, 104. https://doi.org/10.3389/fnmol.2016.00104.

Kasahara, T., Kubota, M., Miyauchi, T., Noda, Y., Mouri, A., Nabeshima, T., Kato, T., and Mouri, A. (2006). Mice with neuron-specific accumulation of mitochondrial DNA mutations show mood disorder-like phenotypes. Mol. Psychiatr. *11*, 577–593. 523. https://doi.org/10.1038/sj.mp.4001824.

Katayama, K., Yamada, K., Ornthanalai, V.G., Inoue, T., Ota, M., Murphy, N.P., and Aruga, J. (2010). Slitrk1-deficient mice display elevated anxiety-like behavior and noradrenergic abnormalities. Mol. Psychiatr. *15*, 177–184. https://doi.org/10.1038/mp.2008.97.

Katayama, K.i., Zine, A., Ota, M., Matsumoto, Y., Inoue, T., Fritzsch, B., and Aruga, J. (2009). Disorganized innervation and neuronal loss in the inner ear of Slitrk6-deficient mice. PLoS One *4*, e7786. https://doi.org/10.1371/journal.pone.0007786.

Kobayashi, K., Ikeda, Y., Haneda, E., and Suzuki, H. (2008). Chronic fluoxetine bidirectionally modulates potentiating effects of serotonin on the hippocampal mossy fiber synaptic transmission. J. Neurosci. *28*, 6272–6280. https://doi.org/10.1523/JNEUROSCI.1656-08.2008.

Kobayashi, K., Ikeda, Y., and Suzuki, H. (2006). Locomotor activity correlates with modifications of hippocampal mossy fibre synaptic transmission. Eur. J. Neurosci. *24*, 1867–1873. https://doi.org/10.1111/j.1460-9568.2006.05079.x.

Kobayashi, K., Mikahara, Y., Murata, Y., Morita, D., Matsuura, S., Segi-Nishida, E., and Suzuki, H. (2020). Predominant role of serotonin at the hippocampal mossy fiber synapse with redundant monoaminergic modulation. iScience *23*, 101025. https://doi.org/10.1016/j.isci.2020.101025.

Konicarova, J., Bob, P., and Raboch, J. (2014). Balance deficits and ADHD symptoms in medication-naive school-aged boys. Neuropsychiatric Dis. Treat. *10*, 85–88. https://doi.org/10.2147/NDT.S56017.

Koob, G.F., Stinus, L., and Moal, M.L. (1981). Hyperactivity and hypoactivity produced by lesions to the mesolimbic dopamine system. Behav. Brain. Res. *3*, 341–359. https://doi.org/10.1016/0166-4328(81)90004-8.

Lein, E.S., Hawrylycz, M.J., Ao, N., Ayres, M., Bensinger, A., Bernard, A., Boe, A.F., Boguski, M.S., Brockway, K.S., Byrnes, E.J., et al. (2007). Genome-wide atlas of gene expression in the adult mouse brain. Nature *445*, 168–176. https://doi.org/10.1038/nature05453.

Leo, D., and Gainetdinov, R.R. (2013). Transgenic mouse models for ADHD. Cell Tissue. Res. *354*, 259–271. https://doi.org/10.1007/s00441-013-1639-1.

Linhoff, M.W., Laurén, J., Cassidy, R.M., Dobie, F.A., Takahashi, H., Nygaard, H.B., Airaksinen, M.S., Strittmatter, S.M., and Craig, A.M. (2009). An unbiased expression screen for synaptogenic proteins identifies the LRRTM protein family as synaptic organizers. Neuron *61*, 734–749. https://doi.org/10.1016/j.neuron.2009.01.017.

Liu, M.-Y., Yin, C.-Y., Zhu, L.-J., Zhu, X.-H., Xu, C., Luo, C.-X., Chen, H., Zhu, D.-Y., and Zhou, Q.-G. (2018). Sucrose preference test for measurement of stress-induced anhedonia in mice. Nat. Protoc. *13*, 1686–1698. https://doi.org/10.1038/s41596-018-0011-z.

Loomis, C., Stephens, A., Janicot, R., Baqai, U., Drebushenko, L., and Round, J. (2020). Identification of MAGUK scaffold proteins as intracellular binding partners of synaptic adhesion protein Slitrk2. Mol. Cell. Neurosci. *103*, 103465. https://doi.org/10.1016/j.mcn.2019.103465.

Maddaloni, G., Migliarini, S., Napolitano, F., Giorgi, A., Nazzi, S., Biasci, D., De Felice, A., Gritti, M., Cavaccini, A., Galbusera, A., et al. (2018). Serotonin depletion causes valproate-responsive manic-like condition and increased hippocampal neuroplasticity that are reversed by stress. Sci. Rep. *8*, 11847. https://doi.org/10.1038/s41598-018-30291-2.

Marteyn, A., Maury, Y., Gauthier, M.M., Lecuyer, C., Vernet, R., Denis, J.A., Pietu, G., Peschanski, M., and Martinat, C. (2011). Mutant human embryonic stem cells reveal neurite and synapse formation defects in type 1 myotonic dystrophy. Cell Stem Cell *8*, 434–444. https://doi.org/10.1016/j.stem.2011.02.004.

Matsumoto, Y., Katayama, K.i., Okamoto, T., Yamada, K., Takashima, N., Nagao, S., and Aruga, J. (2011). Impaired auditory-vestibular functions and behavioral abnormalities of Slitrk6-deficient mice. PLoS One *6*, e16497. https://doi.org/10.1371/journal.pone.0016497.

Mehta, T.R., Monegro, A., Nene, Y., Fayyaz, M., and Bollu, P.C. (2019). Neurobiology of ADHD: a review. Curr. Dev. Disord. Rep. *6*, 235–240. https://doi.org/10.1007/s40474-019-00182-w.

Melo-Felippe, F.B., Fontenelle, L.F., and Kohlrausch, F.B. (2019). Gene variations in PBX1, LMX1A and SLITRK1 are associated with obsessive-compulsive disorder and its clinical features. J. Clin. Neurosci. *61*, 180–185. https://doi.org/10.1016/j.jocn.2018.10.042.

Mertens, J., Wang, Q.-W., Kim, Y., Yu, D.X., Pham, S., Yang, B., Zheng, Y., Diffenderfer, K.E., Zhang, J., Soltani, S., et al. (2015). Differential responses to lithium in hyperexcitable neurons from patients with bipolar disorder. Nature *527*, 95–99. https://doi.org/10.1038/nature15526.

Meziane, H., Ouagazzal, A.M., Aubert, L., Wietrzych, M., and Krezel, W. (2007). Estrous cycle effects on behavior of C57BL/6J and BALB/cByJ female mice: implications for phenotyping strategies. Genes Brain Behav. *6*, 192–200. https://doi.org/10.1111/j.1601-183X.2006.00249.x.

Morimura, N., Yasuda, H., Yamaguchi, K., Katayama, K.I., Hatayama, M., Tomioka, N.H., Odagawa, M., Kamiya, A., Iwayama, Y., Maekawa, M., et al. (2017). Autism-like behaviours and enhanced memory formation and synaptic plasticity in Lrfn2/SALM1-deficient mice. Nat.

Commun. *8*, 15800. https://doi.org/10.1038/ncomms15800.

Mullins, N., Forstner, A.J., O'Connell, K.S., Coombes, B., Coleman, J.R.I., Qiao, Z., Als, T.D., Bigdeli, T.B., Børte, S., Bryois, J., et al. (2021). Genome-wide association study of more than 40,000 bipolar disorder cases provides new insights into the underlying biology. Nat. Genet. *53*, 817–829. https://doi.org/10.1038/s41588-021-00857-4.

Muzerelle, A., Scotto-Lomassese, S., Bernard, J.F., Soiza-Reilly, M., and Gaspar, P. (2016). Conditional anterograde tracing reveals distinct targeting of individual serotonin cell groups (B5–B9) to the forebrain and brainstem. Brain Struct. Funct. *221*, 535–561. https://doi.org/10.1007/s00429-014-0924-4.

Nazzi, S., Maddaloni, G., Pratelli, M., and Pasqualetti, M. (2019). Fluoxetine induces morphological rearrangements of serotonergic fibers in the Hippocampus. ACS Chem. Neurosci. *10*, 3218–3224. https://doi.org/10.1021/acschemneuro.8b00655.

Ozomaro, U., Cai, G., Kajiwara, Y., Yoon, S., Makarov, V., Delorme, R., Betancur, C., Ruhrmann, S., Falkai, P., Grabe, H.J., et al. (2013). Characterization of SLITRK1 variation in obsessive-compulsive disorder. PLoS One *8*, e70376. https://doi.org/10.1371/journal.pone.0070376.

Paxinos, G., and Franklin, K.B.J. (2001). The Mouse Brain in Stereotaxic Coordinates, 2 Edition (Academic Press).

Piton, A., Gauthier, J., Hamdan, F.F., Hamdan, F.F., Lafreniere, R.G., Yang, Y., Henrion, E., Laurent, S., Noreau, A., Thibodeau, P., et al. (2011). Systematic resequencing of X-chromosome synaptic genes in autism spectrum disorder and schizophrenia. Mol. Psychiatr. *16*, 867–880. https://doi.org/10.1038/mp.2010.54.

Purper-Ouakil, D., Ramoz, N., Lepagnol-Bestel, A.-M., Gorwood, P., and Simonneau, M. (2011). Neurobiology of attention deficit/hyperactivity disorder. Pediatr. Res. *69*, 69–76. https://doi.org/10.1203/PDR.0b013e318212b40f.

Reisinger, S.N., Sideromenos, S., Horvath, O., Derdak, S., Cicvaric, A., Monje, F.J., Bilban, M., Häring, M., Glat, M., and Pollak, D.D. (2021). STAT3 in the dorsal raphe gates behavioural reactivity and regulates gene networks associated with psychopathology. Mol. Psychiatr. *26*, 2886–2899. https://doi.org/10.1038/s41380-020-00904-2.

Sadakata, T., Shinoda, Y., Oka, M., Sekine, Y., Sato, Y., Saruta, C., Miwa, H., Tanaka, M., Itohara, S., and Furuichi, T. (2012). Reduced axonal localization of a Caps2 splice variant impairs axonal release of BDNF and causes autistic-like behavior in mice. Proc. Natl. Acad. Sci. U S A *109*, 21104–21109. https://doi.org/10.1073/pnas.1210055109.

Sadakata, T., Washida, M., Iwayama, Y., Shoji, S., Sato, Y., Ohkura, T., Katoh-Semba, R., Nakajima, M., Sekine, Y., Tanaka, M., et al. (2007). Autistic-like phenotypes in Cadps2-knockout mice and aberrant CADPS2 splicing in autistic patients. J. Clin. Invest. *117*, 931–943. https://doi.org/10.1172/JCI29031.

Sakai, K., and Miyazaki, J.i. (1997). A transgenic mouse line that retains Cre recombinase activity in mature oocytes irrespective of the cre transgene transmission. Biochem. Biophys. Res. Commun. *237*, 318–324. https://doi.org/10.1006/bbrc.1997.7111.

Senner, F., Kohshour, M.O., Abdalla, S., Papiol, S., and Schulze, T.G. (2021). The genetics of response to and side effects of lithium treatment in bipolar disorder: future research perspectives. Front. Pharmacol. *12*, 638882. https://doi.org/10.3389/fphar.2021.638882.

Shmelkov, S.V., Hormigo, A., Jing, D., Proenca, C.C., Bath, K.G., Milde, T., Shmelkov, E., Kushner, J.S., Baljevic, M., Dincheva, I., et al. (2010). Slitrk5 deficiency impairs corticostriatal circuitry and leads to obsessive-compulsive-like behaviors in mice. Nat. Med. *16*, 598–602. 591p following 602. 10.1038/nm.2125. https://doi.org/10.1038/nm.2125.

Shum, S.B., and Pang, M.Y. (2009). Children with attention deficit hyperactivity disorder have impaired balance function: involvement of somatosensory, visual, and vestibular systems. J. Pediatr. *155*, 245–249. https://doi.org/10.1016/j.jpeds.2009.02.032.

Smith, E.N., Bloss, C.S., Badner, J.A., Barrett, T., Belmonte, P.L., Berrettini, W., Byerley, W., Coryell, W., Craig, D., Edenberg, H.J., et al. (2009). Genome-wide association study of bipolar disorder in European American and African American individuals. Mol. Psychiatr. *14*, 755–763. https://doi.org/10.1038/mp.2009.43.

Stein, D.J., Costa, D.L.C., Lochner, C., Miguel, E.C., Reddy, Y.C.J., Shavitt, R.G., van den Heuvel, O.A., and Simpson, H.B. (2019). Obsessive-compulsive disorder. Nat. Rev. Dis. Prim. *5*, 52. https://doi.org/10.1038/s41572-019-0102-3.

Stiles, L., Zheng, Y., Darlington, C.L., and Smith, P.F. (2012). The D2 dopamine receptor and locomotor hyperactivity following bilateral vestibular deafferentation in the rat. Behav. Brain. Res. *227*, 150–158. https://doi.org/10.1016/j.bbr.2011.11.006.

Takahashi, H., and Craig, A.M. (2013). Protein tyrosine phosphatases PTPδ, PTPσ, and LAR: presynaptic hubs for synapse organization. Trends. Neurosci. *36*, 522–534. https://doi.org/10.1016/j.tins.2013.06.002.

Takahashi, H., Katayama, K.i., Sohya, K., Miyamoto, H., Prasad, T., Matsumoto, Y., Ota, M., Yasuda, H., Tsumoto, T., Aruga, J., and Craig, A.M. (2012). Selective control of inhibitory synapse development by Slitrk3-PTPδ trans-synaptic interaction. Nat. Neurosci. *15*, S381–S382. https://doi.org/10.1038/nn.3040.

Takashima, N., Odaka, Y.S., Sakoori, K., Akagi, T., Hashikawa, T., Morimura, N., Yamada, K., and Aruga, J. (2011). Impaired cognitive function and altered hippocampal synapse morphology in mice lacking Lrrtm1, a gene associated with schizophrenia. PLoS One *6*, e22716. https://doi.org/10.1371/journal.pone.0022716.

Tekin, M., Chioza, B.A., Matsumoto, Y., Diaz-Horta, O., Cross, H.E., Duman, D., Kokotas, H., Moore-Barton, H.L., Sakoori, K., Ota, M., et al. (2013). SLITRK6 mutations cause myopia and deafness in humans and mice. J. Clin. Invest. *123*, 2094–2102. https://doi.org/10.1172/JCI65853.

Tung, V.W.K., Burton, T.J., Dababneh, E., Quail, S.L., and Camp, A.J. (2014). Behavioral assessment of the aging mouse vestibular system. J. Vector. Ecol. *11*, e51605. https://doi.org/10.3791/51605.

Van Hecke, R., Danneels, M., Dhooge, I., Van Waelvelde, H., Wiersema, J.R., Deconinck, F.J.A., and Maes, L. (2019). Vestibular function in children with neurodevelopmental disorders: a systematic review. J. Autism. Dev. Disord. *49*, 3328–3350. https://doi.org/10.1007/s10803-019-04059-0.

Wood, G.E., Young, L.T., Reagan, L.P., Chen, B., and McEwen, B.S. (2004). Stress-induced structural remodeling in hippocampus: prevention by lithium treatment. Proc. Natl. Acad. Sci. U S A *101*, 3973–3978. https://doi.org/10.1073/pnas.0400208101.

Yamaoka, Y., Abe, C., and Morita, H. (2018). Comparison among ultrasonic, electrical apparatus, and toxic chemicals for vestibular lesion in mice. J. Neurosci. Methods *295*, 58–67. https://doi.org/10.1016/j.jneumeth.2017.11.021.

Yim, Y.S., Kwon, Y., Nam, J., Yoon, H.I., Lee, K., Kim, D.G., Kim, E., Kim, C.H., and Ko, J. (2013). Slitrks control excitatory and inhibitory synapse formation with LAR receptor protein tyrosine phosphatases. Proc. Natl. Acad. Sci. U S A *110*, 4057–4062. https://doi.org/10.1073/pnas.1209881110.

Zuchner, S., Cuccaro, M.L., Tran-Viet, K.N., Cope, H., Krishnan, R.R., Pericak-Vance, M.A., Wright, H.H., Ashley-Koch, A., and Ashley-Koch, A. (2006). SLITRK1 mutations in trichotillomania. Mol. Psychiatr. *11*, 888–889. https://doi.org/10.1038/sj.mp.4001865.

STAR★METHODS

KEY RESOURCES TABLE

REAGENT or RESOURCE	SOURCE	IDENTIFIER
Antibodies		
anti-Slitrk2 (rabbit polyclonal)	this study	N/A
anti-SLITRK2 (goat polyclonal)	R&D Systems	Cat# AF2657; RRID: AB_2190323
anti-Actin (rabbit polyclonal)	Sigma-Aldrich	Cat# A2066; RRID: AB_476693
anti-PSD-95 (clone K28/43)	Antibodies Incorporated	Cat# 75-028; RRID: AB_2292909
anti-VGLUT1 (rabbit polyclonal)	Synaptic Systems	Cat# 135303; RRID: AB_887875
anti-Calretinin (rabbit polyclonal)	Millipore	Cat# ab5054; RRID: AB_2068506
anti-βIII tubulin (clone 5G8)	Promega	Cat# G7121; RRID: AB_430874
anti-SERT (rabbit polyclonal)	Frontier Institute	Cat# HTT-Rb-Af560; RRID: AB_2571775
anti-Tph2 (rabbit polyclonal)	Thermo Fisher Scientific	Cat# PA1-778; RRID: AB_2207687
Donkey Anti-Goat IgG (H+L) Antibody, Alexa Fluor 488 Conjugated	Molecular Probes	Cat# A-11055; RRID: AB_2534102
Donkey Anti-Rabbit IgG (H+L) Antibody, Alexa Fluor 594 Conjugated	Molecular Probes	Cat# A-21207; RRID: AB_141637
Donkey Anti-Mouse IgG (H+L) Antibody, Alexa Fluor 594 Conjugated	Molecular Probes	Cat# A-21203; RRID: AB_141633
Peroxidase-AffiniPure Donkey Anti-Rabbit IgG (H+L)	Jackson ImmunoResearch Labs	Cat# 711-035-152; RRID: AB_10015282
Peroxidase-AffiniPure Goat Anti-Mouse IgG (H+L)	Jackson ImmunoResearch Labs	Cat# 115-035-146; RRID: AB_2307392
Donkey Anti-Mouse IgG (H+L) Antibody, Alexa Fluor 488 Conjugated	Molecular Probes	Cat# A-21202; RRID: AB_141607
Goat Anti-Rabbit IgG (H+L) Antibody, Alexa Fluor 488 Conjugated	Molecular Probes	Cat# A-11008; RRID: AB_143165
Goat Anti-Mouse IgG (H+L) Highly Cross-adsorbed Antibody, Alexa Fluor 594 Conjugated	Molecular Probes	Cat# A-11032; RRID: AB_2534091
Chemicals, peptides, and recombinant proteins		
(2S,2′R,3′R)-2-(2′,3′-dicarboxycyclopropyl) glycine (DCG-IV)	Tocris Bioscience	Cat# 0975
Picrotoxin	FUJIFILM Wako Pure Chemical	Cat# 168-17961
D-2-amino-5-phosphonovaleric acid	Tocris Bioscience	Cat# 0106
Serotonin hydrochloride	Sigma-Aldrich	Cat# H9523
Methylphenidate	Sigma-Aldrich	Cat# M2892
Lithium carbonate-containing (2.4g/kg) diet	Oriental Yeast	N/A
Fluoxetine hydrochloride	Sigma-Aldrich	Cat# F132
Deposited data		
Mouse Brain Atlas	Allen Institute (https://mouse.brain-map.org/experiment/show/69874144)	N/A
Experimental models: Organisms/strains		
Mouse: B6.129(Cg)-Slitrk2^{tm1Jaru}	this study	N/A
Oligonucleotides		
Slitrk2S primer (5'- CCGCCAGCCGGATTTCTAAT-3')	Hokkaido System Science	N/A

(*Continued on next page*)

Continued

REAGENT or RESOURCE	SOURCE	IDENTIFIER
Slitrk2WTAS primer (5'- CACCAGTAGTT TAGCATCTTCAGG-3')	Hokkaido System Science	N/A
Slitrk2KOAS primer (5'- AGAATCCAACC AGTGGGAATGTC-3')	Hokkaido System Science	N/A
Software and algorithms		
Neurolucida (ver. 8)	MBF Bioscience	N/A
SPSS (ver. 16)	SPSS Inc.	N/A
BellCurve for Excel (ver. 3.00)	Social Survey Research Information	N/A
Microsoft Excel (ver. 1808)	Microsoft	N/A

RESOURCE AVAILABILITY

Lead contact

Further information and requests for resources and reagents should be directed to and will be fulfilled by lead contact Jun Aruga (aruga@nagasaki-u.ac.jp).

Materials availability

Mouse line generated in this study is going to be deposited to RIKEN BioResource Research Center (https://web.brc.riken.jp/en/).

Data and code availability

All data reported in this paper will be shared by the lead contact upon request. This paper does not report original code.

EXPERIMENTAL MODEL AND SUBJECT DETAILS

All animal experiments were approved by the institutional ethical committees and were conducted in accordance with the guidelines for animal experimentation in Nagasaki University, Nippon Medical School, and RIKEN. Mice were housed under a 12-h light/dark cycle, with the dark cycle occurring from 8:00 P.M. to 8:00 A.M. Adult male mice were used for all analyses to avoid effects of estrous cycles on behavioral phenotypes in females (Meziane et al., 2007). For behavioral experiments, mice were 7 weeks old at the beginning of the tests and were younger than 16 weeks at the end of the tests except for balance beam test (8–13 months (M)-old) and sucrose preference test (8-10 M-old). 2–4 M-old mice were used for the other experiments otherwise noted. In total, 106 WT mice and 102 KO mice were used for the behavioral analysis and eye movement analysis (Figures 2 and 3, and Table 1), and 48 WT and 52 KO mice were used for drug treatment experiments (Figure 8). Immunostaining analyses in Figures 5A, 5B, 7B, and 7C were carried out using mice experienced the sucrose preference test or the balance beam test (G and H groups in Table 1). The other experiments were carried out using experimentally naïve mice.

METHOD DETAILS

Antibodies

Polyclonal anti-Slitrk2 antibody was raised in a rabbit against peptides corresponding to cytoplasmic region of human SLITRK2 (LEVLEKQTAISQL). Peptides were synthesized and conjugated to keyhole limpet hemocyanin through cysteine added to the N-terminus of the peptide. After rabbits were immunized, antisera were obtained and the antibody was purified by affinity chromatography with the immunized peptide. The specificity of the antibody was validated by immunoblot analysis using KO brain lysates (Figure S10). The following commercial antibodies were used at the indicated dilutions throughout the study: goat anti-SLITRK2 antibody (AF2657, R&D Systems, 1:100), anti-actin antibody (A2066, Sigma-Aldrich, 1:5000), anti-PSD-95 antibody (K28/43, Antibodies Incorporated, 1:600), anti-VGLUT1 antibody (135303, Synaptic Systems, 1:600), anti-Calretinin antibody (ab5054, Abcam, 1:400), anti-βIII tubulin antibody (5G8, Promega, 1:1000), anti-SERT (Slc6A4) antibody (HTT-Rb-Af560, Frontier Institute, 1:300), and anti-Tph2 antibody (PA1-778, ThermoFisher, 1:500). The goat anti-SLITRK2 antibody shows approximately 10% cross-reactivity with recombinant human (rh) SLITRK4 and <2% cross-reactivity with rhSLITRK1 and rhSLITRK5 in direct

enzyme-linked immunosorbent assays (datasheet provided by manufacturer). We verified the signals when using the goat anti-SLITRK2 antibody in immunostaining by comparing them to those in corresponding KO sections.

Western blot analysis

Specimens were homogenized in RIPA buffer (50 mM Tris-HCl pH 8.0, 150 mM sodium chloride, 1% NP-40, 0.5% sodium deoxycholate, 0.1% sodium dodecyl sulfate (SDS), 1 mM ethylenediaminetetraacetic acid (EDTA), and complete protease inhibitor cocktail [Roche Diagnostics]). Approximately 10 μg of the extract was loaded onto a 7.5% SDS-polyacrylamide gel, electrophoresed, and transferred to a polyvinylidene fluoride membrane (Millipore). Rabbit polyclonal anti-Slitrk2 and anti-actin antibodies were used as primary antibodies. After incubation with appropriate secondary antibodies conjugated to horseradish peroxidase, the signals were detected using an ECL Plus kit (GE Healthcare).

Immunofluorescence staining

Immunostaining with anti-SLITRK2, anti-PSD-95 or anti-VGLUT1 antibody was performed as follows: mice were anesthetized with isoflurane and perfused with phosphate buffered saline (PBS) from the left ventricle to the right atrium for 1 min. Brains were immediately dissected and frozen on dry ice. Thereafter, 12-μm sections were prepared using Leica CM3050S. The sections were dried, immersed in 4% paraformaldehyde (PFA), incubated in 0.1 M sodium phosphate for 3 or 30 min at 4°C, and rinsed with PBS.

Immunostaining with anti-SERT antibody or anti-Tph2 antibody was performed as follows: mice were anesthetized with isoflurane, perfused with 4% PFA in 0.1 M sodium phosphate (pH 7.4) at a rate of 6.5 mL/min for 3 min, and brains were excised and postfixed in the same solution for 4 h at room temperature with gentle agitation. The brains, including the raphe nuclei, were cut into 4-mm sections using Rodent Brain Matrix (ASI Instruments) and immersed in 20% sucrose in PBS for 16 h. After being embedded in OCT compound (Sakura Finetek), 20-μm serial coronal sections encompassing the bregma (−3 to −5.5 mm) were prepared. Every fourth section was subjected to immunostaining. The sections were immersed in PBS after storage at −30°C.

After being blocked with blocking buffer (2% normal goat or 5% donkey serum, 0.1% Triton X-100, and PBS) for 0.5 or 1 h, the sections were incubated with primary antibody diluted in the blocking buffer for 12–72 h. The bound antibodies were detected using Alexa488 or Alexa594-conjugated secondary antibodies (Jackson ImmunoResearch). Images were acquired using the Keyence BZ-X700, Zeiss LSM800, Olympus FV1000, or Leica MZ-16FA microscope. Quantification of PSD-95-, VGLUT1-, SERT-, and Tph2-immunopositive signals was performed using particle analysis function of the ImageJ software (https://imagej.nih.gov/ij/). For the analysis of PSD-95 and VGLUT1 signals, 101.41 × 101.41 μm (512 × 512 pixel) images were captured with ×63 objective lens at the scanning speed of 0.02 ms/pixel using LSM800. Two independent images were obtained from one parasagittal section (lateral to 0.60–0.72 mm, (Paxinos and Franklin, 2001)). The threshold values were set to see the punctate signals most clearly and uniform values were used for PSD-95 and VGLUT1 respectively. For the analysis of SERT and Tph2 signals, images were captured by at ×20 objective lens using BZ-X700. The image collection and target region selection were carried out in a genotype-blinded manner. Target particle size range was set to 0.3–0.8 μm^2 (PSD-95, VGLUT1), 0.1–0.8 μm^2 (PSD-95/VGLUT1 double-positive) or 16–225 μm^2 (Tph2, SERT). The estimated total serotonergic cell count in a raphe nucleus was calculated by multiplying the total particle number by 4.

Generation of Slitrk2-null mutant mice

Slitrk2-null mutant mice were generated as described previously (Katayama et al., 2010). Briefly, to construct the *Slitrk2* targeting vector, overlapping *Slitrk2* genomic clones were isolated from a phage library derived from 129SV mice (Stratagene, La Jolla, CA). The targeting construct contained the 1.4-kb 5' and 5.7-kb 3' homology regions, and the 5.8-kb fragment containing the open reading frame of *Slitrk2* was replaced with the phosphoglycerol kinase (PGK)–neo expression cassette flanked by a *loxP* sequence. E14 embryonic stem (ES) cells were electroporated with the targeting construct and selected with G418. Drug-resistant clones were analyzed by Southern blotting. *Eco*RV-digested genomic DNA were hybridized with a 1.0-kb 5' genomic fragment that corresponded to the genomic sequence outside the targeting vector and a 0.6-kb *Pst*I PGK–neo probe, respectively. Chimeric mice were generated by the injection of targeted ES cells into C57BL/6J blastocysts. To excise the PGK–neo cassette, germline-transmitted mice were first mated with mice transgenic for Cre recombinase under the control of the cytomegalovirus immediate

early enhancer–chicken β-actin hybrid (CAG) promotor (Sakai and Miyazaki, 1997). Correct excision of the PGK–neo cassette was confirmed by Southern blot. The resultant mutant allele (*Slitrk2*$^{-}$) contained a single *loxP* sequence in place of the targeted 5.8-kb region that does not contain any known functional non-coding RNAs other than Slitrk2 gene in search of mouse genome (GRCm39) using GENCODE M29 database (Frankish et al., 2021). It is highly probable that the phenotypes caused by the mutation reflect the lack of Slitrk2 protein. Mice carrying *Slitrk2*$^{-}$ were backcrossed to C57BL/6J for more than 8 generations before analysis. Genotyping of progenies was performed by Southern blotting or PCR analysis of DNA isolated from tail samples; PCR primers used were Slitrk2S (5'- CCGCCAGCCGGATTTCTAAT-3'), Slitrk2WTAS (5'- CACCAGTAGTTTAGCATCTTCAGG-3'), and Slitrk2KOAS (5'- AGAATCCAACCAGTGGGAATGTC-3').

Home cage activity

Spontaneous activity of mice in their home cage was measured using the 24-channel ABsystem 4.0 (Neuroscience, Tokyo, Japan). Cages were kept individually into the stainless-steel compartments of the breeding rack (JCL, Tokyo, Japan). A cage-top external infrared light sensor detecting horizontal and vertical activity was used to detect mice movement in their home cage. Home cage activity was measured for 1 week from 4:00 P.M. on day 1–4:00 P.M. on day 8.

Open field test

The open field test was performed as previously described (Morimura et al., 2017). Each mouse was placed in the center of an open-field apparatus (50 × 50 × 40 [H] cm) illuminated by light-emitting diodes (70 lx at the center of the field) and allowed to move freely for 15 min. Distance traveled (cm) and time spent (%) in the center area of the field (30% of the field) were adopted as the parameters and relevant data were collected every minute. Data were collected and analyzed using Image J OF4 (O'Hara, Tokyo, Japan).

Elevated plus maze test

Each mouse was placed on the central square, facing an open arm of the plus-maze (central platform: 5 × 5 cm, two open arms: 25 × 5 × 0.5 cm, two enclosed arms: 25 × 5 × 15 cm, O'Hara). Mouse behavior was recorded by an overhead video camera during the 5-min test period. Data analysis was performed automatically using ImageJ EPM (O'Hara).

Light-dark box test

The apparatus used for the light-dark box test consisted of a cage (20 × 40 × 20 cm) divided into two sections of equal size by a partition containing a door (O'Hara). One chamber was brightly illuminated (250 lx), whereas the other chamber was dark. Mice were placed in the light box and allowed to move freely between two two chambers with the door open for 10 min. The total number of transitions, percent time spent in the light side, and percent distance traveled in the light side were recorded and calculated using ImageJ LD4 (O'Hara).

Marble burying test

Transparent plastic cages (25 × 18 × 15 cm) were filled with 4-cm deep white paper bedding material (Paperclean, Japan SLC). Mice were placed individually in the test cages for 20 min (habituation trial) and thereafter, returned to their home cages. Fifteen blue glass marbles (17-mm diameter) were evenly set at 5-cm intervals on the surface of the bedding material in the habituated cages. Thereafter, mice were again placed in the habituated test cage for 20 min (test trial). During both the trials, the test cage with the mouse was set in the infrared beam apparatus (SCANET, MELQUEST, Toyama, Japan) to measure activity. After 20 min, marbles that were more than two-thirds covered with Paperclean were counted as buried marbles.

Hole board test

The testing apparatus consisted of a gray plastic box (50 × 50×40 [H] cm) with four equally separated holes (3-cm diameter with infra-red sensor) on the floor (Model ST-1/WII, Muromachi-Kikai, Tokyo, Japan). The field was illuminated by fluorescent light (180 lx, at the center of the field). The behavior of each mouse was monitored using a CCD camera located approximately 1.5 m above the field. In the test, mice were individually introduced into the center of the field and were then allowed to explore freely for 5 min. Data were collected and analyzed using a CompACT VAS system (Muromachi-Kikai).

Forced swim test

The test was conducted as previously described (Katayama et al., 2010). Each mouse was placed for 6 min in a glass cylinder (height: 30 cm, diameter: 10 cm) containing 20 cm of water maintained at 23°C-25°C. The duration of immobility was recorded during the last 3 min of the test period.

Tail suspension test

The test was conducted as previously described (Katayama et al., 2010). Mice were attached to a wire using an adhesive tape placed approximately 1.5 cm from the tip of the tail and were suspended 30 cm above the floor. The duration of immobility was recorded for 5 min.

Sucrose preference test

The test was done according to Liu et al. (2018) with slight modification. Mice were first adapted to isolation rearing in a cage with two bottles for liquid supply (Drinko-Measurer, O'hara), one containing sucrose water (1% (wt/vol)) and one containing regular water for 48 h. On the test day, mice were deprived of both food and water from 9:00 A.M. The test was started by placing the sucrose water bottle and the regular water bottle at 6:00 P.M. and ended by removing the two bottles at 9:00 A.M. on the next day. The net consumption of the liquids was measured by weighing the bottles before and after the tests.

Rotarod test

In the rotarod test (MK-610A, Muromachi Kikai), the rotating rod was accelerated from 4 to 40 rpm over the course of 5 min. Each mouse was placed on the rod, and once they were balanced, the rod accelerated. The time at which the mouse fell from the rod was recorded. Each mouse went through three consecutive trials on 2 consecutive days.

Social behavior tests

Reciprocal social interaction among freely moving mice was assessed using the open field apparatus (60 × 60 × 60 [H] cm; O'Hara) with an automatic video tracking device and the NIH Image SI 1.10 software (O'Hara) as described (Sadakata et al., 2007). Each mouse was placed and habituated in the open field apparatus for 20 min per day for 4 days. Two genetically identical mice (ten pairs of each genotype) that had been housed separately were placed at the opposite corners of the apparatus and allowed to move freely for 10 min. Social interaction was analyzed by counting the number of particles in each frame—the presence of two particles indicated no contact with each other and the presence of one particle indicated contact each other. The total number and duration of contact were measured and analyzed. The social preference test was performed in the same open field apparatus as described (Sadakata et al., 2012) with minor modifications. One small vacant cage was placed in one corner and another cage with a stranger C57BL/6J mouse was placed in the neighboring corner. Each mouse was placed into the open field apparatus on the opposite side of the cages and allowed to move freely for 10 min. The time spent in two corner squares containing the cages within subdivision (17.7 × 17.7 cm^2) was measured.

Tests for startle response, wire hanging, and grip strength

Tests for startle response and its prepulse inhibition and water maze test were performed as described (Morimura et al., 2017). In the wire hanging test, mice were placed on the cage top, which was then inverted and suspended above the cage; the latency to when the mouse fell was recorded. Three trials were conducted in succession. In grip strength test, the grasping applied by the mouse on a grid connected to a sensor (Muromachi Kikai) was assessed. Three trials were conducted in succession to measure forelimb strength.

Water maze test and fear conditioning test

Hole board test, water maze test, and fear conditioning test was carried out as described (Takashima et al., 2011).

Balance beam test

Mice were initially trained to walk across a wooden beam (15-mm-wide square beam, elevated 60 cm above the floor) for 4 consecutive days (four trials/day). Testing session was conducted on the next day using 9- and 5-mm-wide square beams. Time to traverse each beam was recorded for each trial with a 60-s

maximum cutoff. Three consecutive trials using 9- and 5-mm beams were conducted and video recorded. The average of the three trials was used for data analysis. Frequency of hindlimb slipping was counted on the video record by an observer.

VOR and OKR eye movements

Eye movement was measured using the infrared TV method as described previously (Matsumoto et al., 2011). Under isoflurane (Escain, Mylan- Japan, Tokyo, Japan) anesthesia and aseptic conditions, a platform for head fixation was made on the mouse cranial bone using synthetic resin (Superbond C & B, Sun Medical, Tokyo, Japan) and one 15-mm stainless bolt. Two days after surgery, mice were mounted on a turntable surrounded by a checked-pattern (check size: 4°) screen (diameter: 60 cm; height: 60 cm), with the head fixed and the body loosely restrained in a plastic cylinder. Horizontal VOR and horizontal OKR eye movements were measured. The VOR was measured in the dark by oscillating the sinusoidal turntable at a frequency of 0.11–0.50 Hz and a peak-to-peak amplitude of 10° in the plane parallel to the bilateral horizontal semicircular canals. The OKR was measured in the light by oscillating the sinusoidal screen at a frequency of 0.11–0.33 Hz and a peak-to-peak amplitude of 10°–20° (maximum screen velocity: 3.5°–10.5°/s) in the same plane. More than ten cycles of the evoked horizontal (VOR and OKR) eye movements free from artifacts due to blinks and saccades were averaged, and the mean amplitude and phase were calculated by a modified Fourier analysis (Jastreboff, 1979). A gain of the eye movement was defined as the ratio of the peak-to-peak amplitude of eye movements to that of the turntable or screen oscillation. The phase was defined as 0° when the peak of the eye movement was opposite to the peak of turntable oscillation in the VOR and when the peak of the eye movement matched the screen oscillation in the OKR.

Electrophysiology

The analysis was performed as described (Kobayashi et al., 2008, 2020). Mice aged 11–28 weeks were decapitated under deep halothane anesthesia, and both hippocampi were isolated. Transverse hippocampal slices (380 μm) were cut using a tissue slicer (7000 smz, Campden Instruments Ltd., Leics., UK) in ice-cold saline (see below). Thereafter, tissue slices were incubated for 30 min at 30°C in saline and maintained in a humidified interface holding chamber at room temperature before use. Electrophysiological recordings were performed in a submersion-type chamber maintained at 27.0°–27.5°C and superfused at 2 mL/min with recording saline composed of (in mM): NaCl, 125; KCl, 2.5; $NaH2PO_4$, 1.0; $NaHCO_3$, 26.2; glucose, 11; $CaCl_2$, 2.5; and $MgCl_2$, 1.3 (equilibrated with 95% O_2/5% CO_2). Field excitatory postsynaptic potentials (EPSPs) arising from the mossy fiber synapses were evoked by stimulating the dentate granule cell layer with bipolar tungsten electrodes and recorded from the stratum lucidum of CA3 using a glass pipette filled with 2 M NaCl. The amplitude of field EPSPs was measured with a 0.5-ms window positioned at 70–80% of the peak of baseline field EPSPs. A criterion used to identify the mossy fiber input was >85% block of EPSP by an agonist of group II metabotropic glutamate receptors, (2S,2′R,3′R)-2-(2′,3′-dicarboxycyclopropyl) glycine (DCG-IV, 1 μM; Tocris Bioscience; Bristol, UK). Single electrical stimulation was delivered at a frequency of 0.05 Hz. Recording of field EPSPs at the medial perforant path-granule cell synapse was performed by placing stimulating and recording electrodes in the middle third of the molecular layer in the dentate gyrus, and synaptic inhibition was blocked by picrotoxin (100 μM; FUJIFILM Wako Pure Chemical Industries, Ltd; Osaka, Japan). LTP was induced by tetanic stimulation (100 Hz, 0.5 s) repeated three times. Input-output relationship was examined in the presence of D-2-amino-5-phosphonovaleric acid (Tocris). Serotonin hydrochloride was purchased from Sigma-Aldrich and directly dissolved in the dialysate.

Morphological analysis

For electron microscopic analysis, anesthetized mice (10 weeks old, three pairs of male Slitrk2 KO and WT mice) were perfused with 2% PFA/2.5% glutaraldehyde in 0.1 M sodium phosphate buffer (pH 7.4). Brains were sectioned at 200 μm on a Vibratome (VT1000/EM UC6, Leica Biosystems, Nussloch, Germany), osmicated with 1% OsO_4 in phosphate buffer, dehydrated through a gradient series of ethanol, and embedded in epoxy resin (Epon 812, TAAB Laboratories Equipment Ltd, Berkshire, England). Ultra-thin sections of the hippocampus (70 nm) were cut with an ultramicrotome (EM UC6, Leica), collected on 200-mesh uncoated copper grids, and counterstained with uranyl acetate and lead citrate. CA3 stratum lucidum were examined electron microscopically (Tecnai 12, FEI, Eindhoven, Netherlands). Photographic images were acquired using the digital camera (Tem Cam F416, TVIPS, Gauting, Germany) attached to the electron microscope. For fine structural analysis, high resolution images (1.7 nm/pixel, 6.8 × 6.8 μm^2) were captured at ×9300 microscopic magnification. The presynaptic area, synaptic cleft width, postsynaptic density, and synaptic vesicle-related parameters were manually measured using Neurolucida software (MBF Bioscience).

For Golgi staining, brains of three pairs of male Slitrk2 WT and KO littermates (age, 8 weeks) were stained using the modified Golgi-Cox impregnation of neurons performed with an FD Rapid GolgiStain kit (FD NeuroTechnologies). We prepared coronal sections (thickness, 100 μm) and examined the area of the molecular layer of the dorsal hippocampal dentate gyrus. Thirty dendritic branches were analyzed by manually tracing with the Neurolucida software (MBF Bioscience).

Neurochemical analysis

Samples were punched from the prefrontal cortex, striatum, hippocampus, amygdala and nucleus accumbens of coronally sliced frozen brain sections and analyzed as previously described (Kabayama et al., 2013). Monoamine content is presented corrected for protein content and internal standard.

Drug administration

Methylphenidate (Sigma-Aldrich) was dissolved in saline and administered intraperitoneally to mice (5 mg/kg of methylphenidate) immediately before the open field test. As controls, gender-matched littermates were injected with the same volumes of saline. Lithium was administered in the diet at a concentration of 2.4 g Li_2CO_3 per 1 kg dry food (Oriental Yeast Co., Tokyo, Japan) for 4 weeks. This treatment regimen is known to result in a plasma lithium level of 0.63 $\pm$ 0.17 mM, comparable to human therapeutic range (Kasahara et al., 2006). Control mice were administered the normal diet. Owing to the well-known side effects of lithium (such as polyuria and polydipsia), mice were supplied with saline in addition to water to prevent possible electrolyte imbalance. For chronic treatment of fluoxetine (Sigma-Aldrich), mice were first individually maintained in the aforementioned home cages for spontaneous activity measurement for the first 8 days. Thereafter, mice were administered 10 mg/kg/day of fluoxetine through drinking water for 10 days. The activity was continuously monitored throughout the experimental period.

QUANTIFICATION AND STATISTICAL ANALYSIS

Statistical analyses were performed using the SPSS statistical package (ver. 16, SPSS Inc.) and BellCurve for Excel (Social Survey Research Information Co., Ltd). Parametric data were analyzed using the two-tailed unpaired Student's *t* test, and non-parametric data were analyzed by using the Mann–Whitney's *U*-test. The effects of factors were analyzed using multifactorial ANOVA. Multiple test correction was done by Benjamini-Hochberg (BH) post-hoc tests. Differences were considered statistically significant when $p < 0.05$. Results are presented as mean with standard deviation (SD), otherwise stated. In the Results section, percentage values are calculated as $(KO_{mean} - WT_{mean}) / WT_{mean} \times 100$, and p-values are values obtained through two-tailed unpaired t-test between WT and KO mice (n = mouse number), otherwise stated.